SANDIA REPORT

SAND97–1595 • UC–000
Unlimited Release
Printed July 1997

Conceptual Design for an Electron-Beam Heated Hypersonic Wind Tunnel

Ronald J. Lipinski, Ronald P. Kensek

Prepared by
Sandia National Laboratories
Albuquerque, New Mexico 87185 and Livermore, California 94550

Sandia is a multiprogram laboratory operated by Sandia Corporation, a Lockheed Martin Company, for the United States Department of Energy under Contract DE-AC04-94AL85000.

Sandia National Laboratories

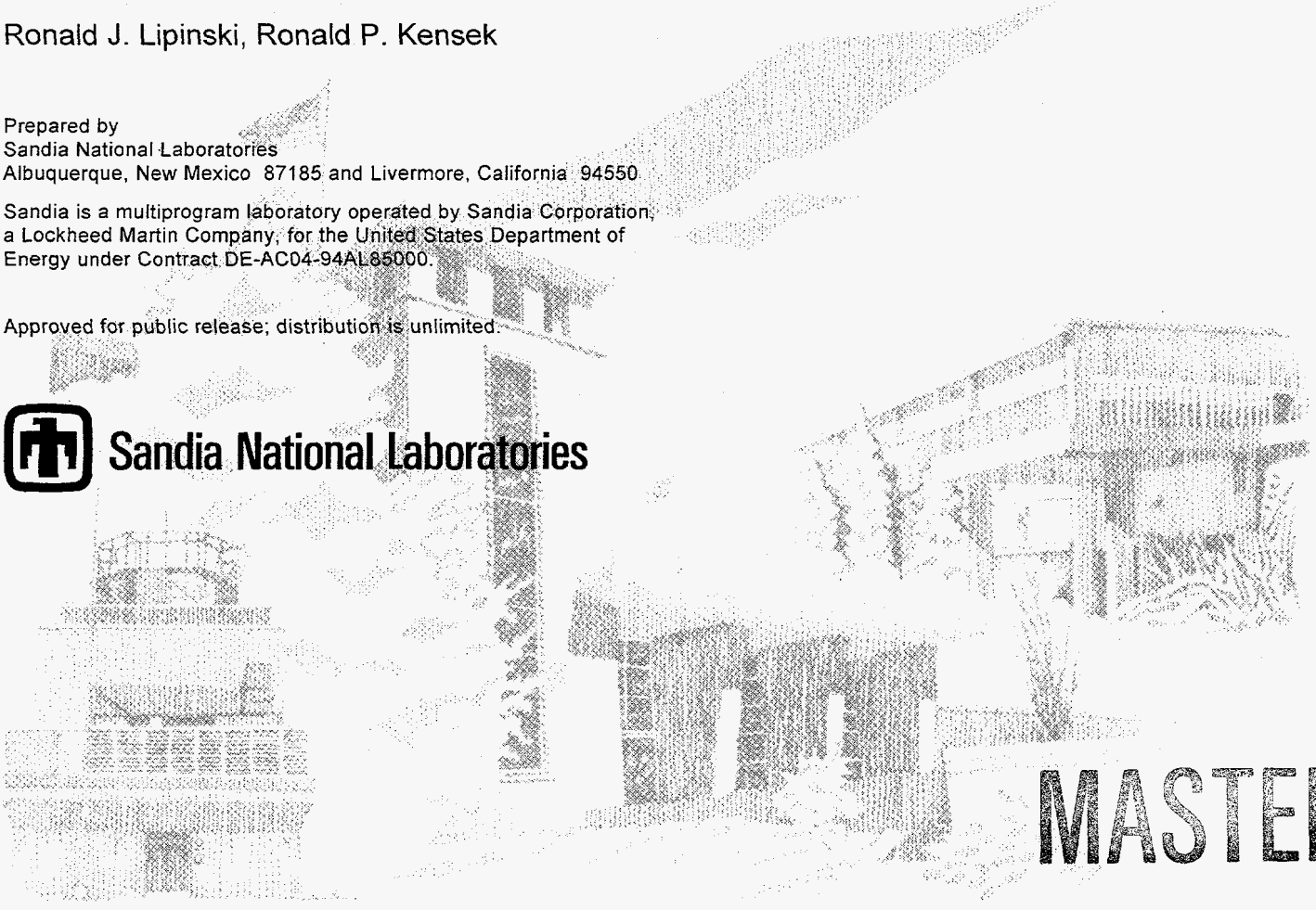

Issued by Sandia National Laboratories, operated for the United States Department of Energy by Sandia Corporation.

Available to DOE and DOE contractors from
Office of Scientific and Technical Information
P.O. Box 62
Oak Ridge, TN 37831

Prices available from (615) 576-8401, FTS 626-8401

Available to the public from
National Technical Information Service
U.S. Department of Commerce
5285 Port Royal Rd
Springfield, VA 22161

NTIS price codes
Printed copy: A04
Microfiche copy: A01

SAND97-1595
Unlimited Release
Printed July 1997

Conceptual Design for an Electron-Beam Heated Hypersonic Wind Tunnel

Ronald J. Lipinski
Nuclear Technology and Research Department

Ronald P. Kensek
Simulation Technology Research Department

Sandia National Laboratories
P. O. Box 5800
Albuquerque, New Mexico 87185-1146

Abstract

There is a need for hypersonic wind-tunnel testing at about Mach 10 and above using natural air and simulating temperatures and pressures which are prototypic of flight at 50 km altitude or below. With traditional wind-tunnel techniques, gas cooling during expansion results in exit temperatures which are too low. Miles, et al.[1], have proposed overcoming this difficulty by heating the air with a laser beam as it expands in the wind-tunnel nozzle. This report discusses an alternative option of using a high-power electron beam to heat the air as it expands.

In the e-beam heating concept, the electron beam is injected into the wind-tunnel nozzle near the exit and then is guided upstream toward the nozzle throat by a strong axial magnetic field. The beam deposits most of its power in the dense air near the throat where the expansion

(Abstract continued on next page.)

rate is greatest. A conceptual design is presented for a large-scale system which achieves Mach 14 for 0.1 seconds with an exit diameter of 2.8 meters. It requires 450 MW of electron beam power (5 MeV at 90 A). The guiding field is 500 G for most of the transport length and increases to 100 kG near the throat to converge the beam to a 1.0-cm diameter. The beam generator is a DC accelerator using a Marx bank (of capacitors) and a diode stack with a hot cathode. The

beam is injected into the wind-tunnel nozzle at the low-pressure end through a foilless window, with differential pumping and cryopanels used to maintain the vacuum in the diode region.

A second conceptual design also is presented for a pilot-scale system which achieves Mach 12 for 1 second with an exit diameter of 0.33 meters. It requires 25 MW of beam power (5 MeV at 5 A). The guiding field is 3 kG for most of the transport length and increases to 200 kG near the throat to converge the beam to a 0.24-cm diameter. The e-beam accelerator is similar to the large-scale design.

The behavior of the beam as it deposits its energy near the nozzle throat is modeled in detail using a trajectory code which follows 200,000 sample electrons. Spiraling of the electrons around the guiding field line, intense scattering, and generation of secondary electrons are included in the modeling. A second model is used to determine the effects of gas ionization by the beam, recombination, and chemical interactions in the gas flow. This model predicts that the mole fractions of NO and NO_2 at the nozzle exit are less than 0.1% each.

A brief look at the required accelerator, magnets, and power supply is made, and it is concluded that there are no show-stoppers in these areas. A crude cost estimate is made for development and construction of the e-beam system (accelerator, vacuum system, magnets, power supplies, controls, and diagnostics). Estimated costs for the large-scale and the pilot-scale e-beam systems are $95 M and $65 M, respectively.

Acknowledgments

This work supported by the U.S. Air Force under a contract from the Arnold Engineering Development Center and by the U.S. Department of Energy under contract DE-AC04-94AL85000. The authors also wish to thank Prof. R. Miles and Dr. W. Lempert of Princeton University for their support, R. Anderson of Princeton for the pilot-scale hypersonic modeling, M. Kushner of the University of Illinois for the chemical modeling, and M. Buttram at Sandia National Laboratories for advice on accelerator design.

Intentionally Left Blank

Contents

1. Introduction

The U.S. has a need for an experimental wind tunnel facility in the Mach-14 regime in order to maintain the cutting edge in aerospace technology. Small-scale facilities using simulant gases (e.g. helium or hydrogen) can achieve up to Mach 20, but can not provide the fidelity in gas constituents or scale which is needed for hypersonic engine or aircraft development. Heating and ablation of leading edges of airfoils is sensitive to the actual gas mixture. Combustion in engines is particularly sensitive to gas composition and temperature. It is essential to duplicate, or to simulate as closely as possible, the velocity, gas composition, temperature, and pressure prototypic of Mach-14 flight at about 50 km (170,000 ft) altitude or below, and to do so with a nozzle cross-section large enough for engine development.

The traditional approach for making a wind tunnel is to start with a high-pressure, high-temperature plenum, and then expand the gas at a balanced rate (to avoid shocks or choking) until the desired Mach number is achieved. There must be sufficient internal energy and pressure in the plenum gas to allow for cooling during expansion and still end up at the desired final temperature and pressure. The fundamental difficulty in achieving prototypic conditions at Mach 14 by using this traditional technique is that it requires an initial temperature and pressure which leads to unacceptable chemical constituents and intolerable heating of the nozzle throat.

The solution to this dilemma proposed by Miles, et al,[1, 2] is to use a cooler gas in the plenum and then heat it in the expansion nozzle as it travels. Specifically, they propose using a very high-power laser tuned to a wavelength which can be readily absorbed by the gas. An HF laser (2.76-μm wavelength) is suggested as a good candidate since that wavelength can be absorbed by the CO_2 in the air, and the CO_2 can transfer that energy to the rest of the air before the gas travels very far. However, for a 3-m diameter exit region, the laser needs to be 400 MW for at least 0.1 seconds. This is a very high power for such a long duration, and might be too expensive.

Since laser beams are a very expensive form of energy one would expect to save money and reduce risk if electron beams could be used to heat the air instead. This is especially true since electron beams can be generated with typically 80% electrical efficiency, compared with 1-4% electrical efficiency for the best electrically driven lasers, and 10-20% efficiency for chemically-driven lasers. In addition, the hardware to generate an electron beam is less complex and costly than for a laser beam, and the absorption in air occurs much more readily, without tuning to a particular energy.

As an alternative to a laser beam, this report suggests using an electron beam (which fills the nozzle) to heat the air. There are questions about how to generate such a beam, how to guide it through the wind-tunnel nozzle, and the effects of chemical interactions induced by the beam. All these issues are addressed in this report.

2. Functional Requirements for E-Beam Heating

The electron beam must meet the following criteria, or "functional requirements", in order to successfully heat the air in the wind-tunnel nozzle:

1. Provide sufficient total power and duration. Typically this is 400 MW for 0.1 seconds for a large-scale wind tunnel and 20 MW for 1.0 seconds for a pilot-scale wind tunnel.
2. Penetrate uniformly into the gas in the nozzle near the throat.
3. Heat the gas in the nozzle at a rate consistent with nozzle expansion to provide near constant temperature or constant entropy without creating a reverse pressure gradient.
4. Avoid melting the nozzle wall.
5. Avoid generation of non-prototypic chemicals.

All this should be accomplished using existing or near-term technologies.

3. Electron-Beam Energy-Deposition Characteristics

Electrons deposit energy in air and in solids by a combination of atomic excitation, ionization, and Bremsstrahlung x-ray production. Figure 3.1 shows the range of electrons in air as a function of initial electron energy.[3] The range is given in terms of "areal density" (g/cm^2), which is equivalent to the range in cm for air at 820 times standard density. The energy deposition rate also is given, and is nearly constant, which is different than for a laser beam. The energy deposition from a laser beam is dominated by the photoelectric effect. The photons are destroyed when they lose their energy, so there are fewer and fewer of them as the beam propagates. Thus, the deposition form a laser beam decreases exponentially as the beam penetrates the air, while the deposition from an electron beam is much more uniform as the electrons slow down over their range.

The dashed curve shows the energy deposition including Bremsstrahlung. . For an electron energy of 5 MeV, the Bremsstrahlung yield is only 2.2% in air. Bremsstrahlung is not significant in air because the constituents all have low atomic numbers.

For electron energies above 0.5 MeV, the range is approximately

$$R = (0.5\ \mathrm{g/cm^2})\frac{E_e}{1\ \mathrm{MeV}} \qquad (3.1)$$

where the range is given in terms of the mass per unit area penetrated and E_e is the initial energy of the electron. (Mass per unit area is called "areal density".) This formula is essentially independent of material that the beam passes through, and the deposition rate is approximately uniform over the range (except at the very end when the energy drops below 0.5 MeV).

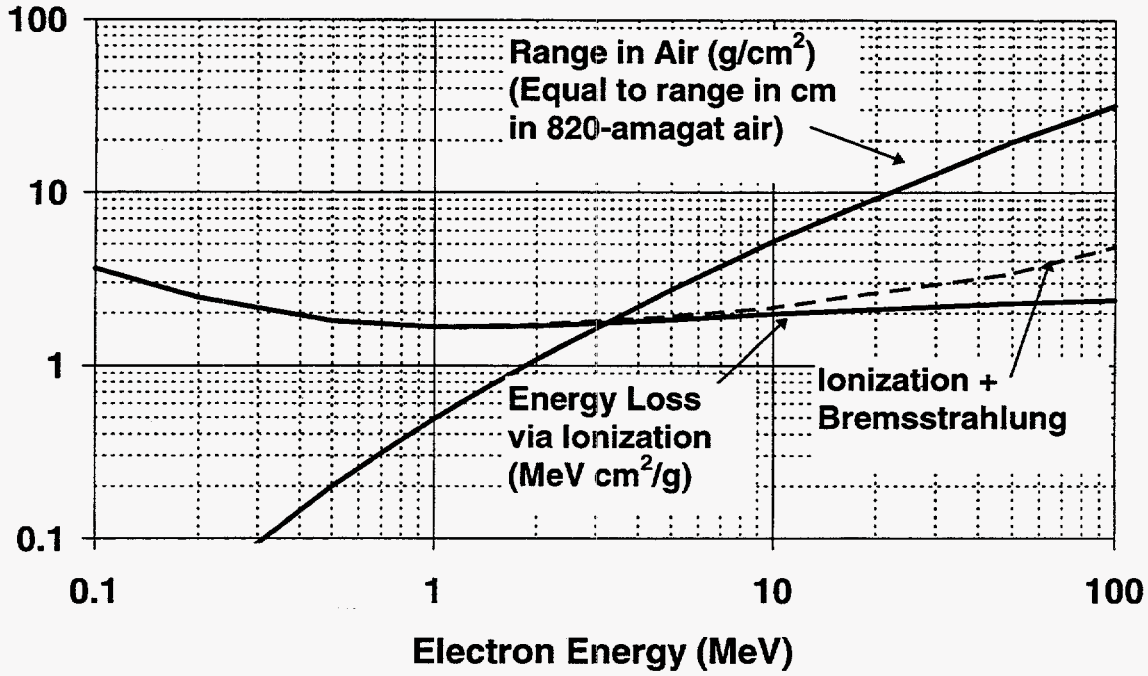

Figure 3.1. Range of electrons in air, and energy deposition rate.

Figure 3.2 shows the deposition rate (per unit length) for an electron beam in water as calculated in detail by the CYLTRAN code of the ITS suite. As expected, it is primarily flat, but there also is a slight tail caused by random variations in the electron paths and a modest peak due to backscattered electrons. The behavior in air is similar when scaled by the density.

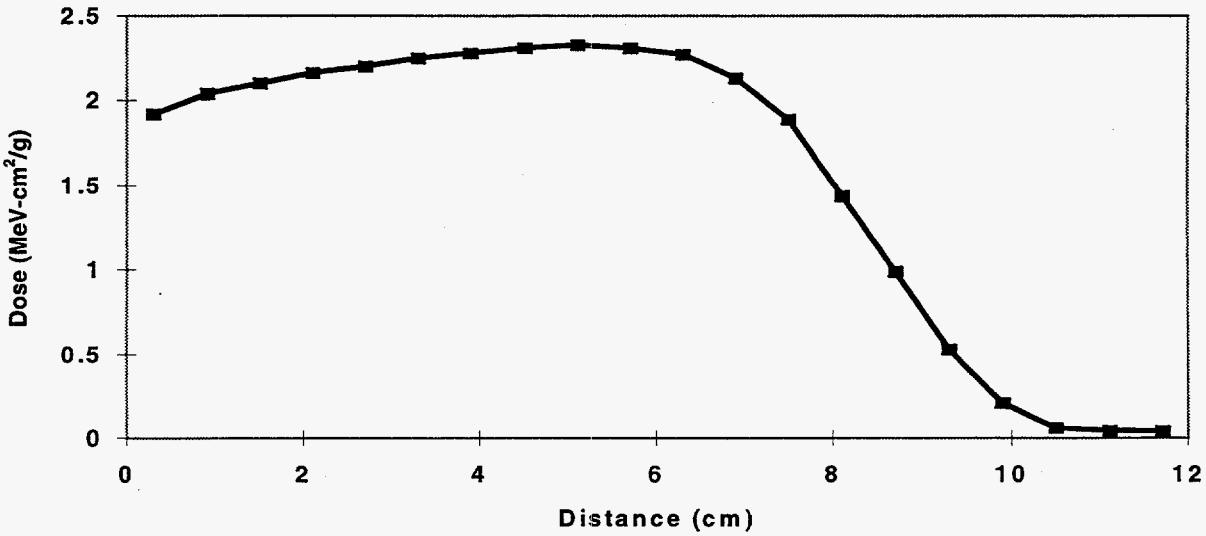

Figure 3.2. Energy deposition rate for electrons in water as calculated by the CYLTRAN code.

4. Configuration Options for E-Beam Heating

4.1 Transverse Beam

Since our geometry is thin compared to the range of selected electrons, one option for heating the wind-tunnel air is to establish a beam just downstream of the throat which penetrates the nozzle wall transversely, as shown in Figure 4.1. Unfortunately, wall heating is a problem in this configuration.

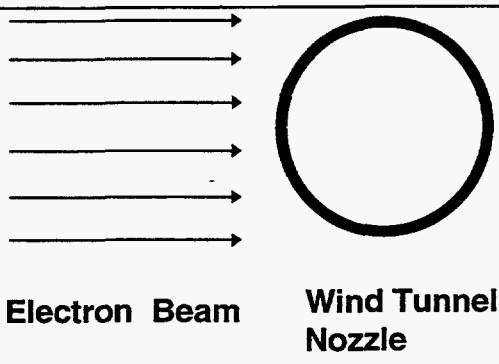

Figure 4.1. Cross section of wind-tunnel nozzle with transverse electron beam. Wall heating is a problem.

The energy deposition rate of an electron in matter (as implied by equation 1) is about 0.2 MeV for each 1 kg/m^2 penetrated. This converts to a beam deposition rate of 200 kW/kg for each A/m^2 of current:

$$S = 2.0\text{x}10^5 \frac{\text{W/kg}}{\text{A/m}^2} \qquad (4.1)$$

The heating rate in matter is then

$$\frac{dT}{dt} = \frac{SI}{AC_p} \qquad (4.2)$$

In order to deliver 400 MW over a length of 1 meter, the beam would need to be approximately 5 MeV and 260 A (allowing for penetration losses in the wall). Such a beam is feasible, but the wall would heat 660,000 K in 0.1 seconds, which is way beyond acceptability. The details for the transverse-beam option are shown in Table 4.1. The fundamental difficulty is that the beam must be intense enough to raise the air temperature by the equivalent of about 1000 K (which is offset by expansive cooling) in the time it takes the air to move a meter (about 0.0005 sec). This is fine for the air which is replaced every 0.0005 seconds, but not so fine for the wall which just sits there. So we need a different approach.

Table 4.1. Conditions for heating with a transverse e beam.

Beam Size	2 cm x 50 cm
Axial Location	0 to 0.5 m
Gas Thickness	8 kg/m^2
Wall Thickness	10 kg/m^2 ?
Voltage	5 MV
Beam Range	27 kg/m^2
% Power in Gas	30%
Current	260 A
Power	1300 MW
Power in Gas	400 MW
Wall Heating Rate	6600 °/ms
Time to Melt	< 1 ms

4.2 Axial Beam with Annular Window

One solution to the wall-heating problem is to spread the beam over a much larger area so that the heating rate is greatly reduced. This can be done at the far end of the nozzle where the diameter is much larger. An annular beam can be injected through a thin section of the wall (called a "window" since it is thin enough to be as transparent to electrons as glass is to light). The wall heating will be minimized if the beam passes through perpendicularly, so a step in the nozzle diameter could be used, as shown in Figure 4.2. If this step is only slightly in front of the test article, the shock from it (in the air) will not impinge on the test article.

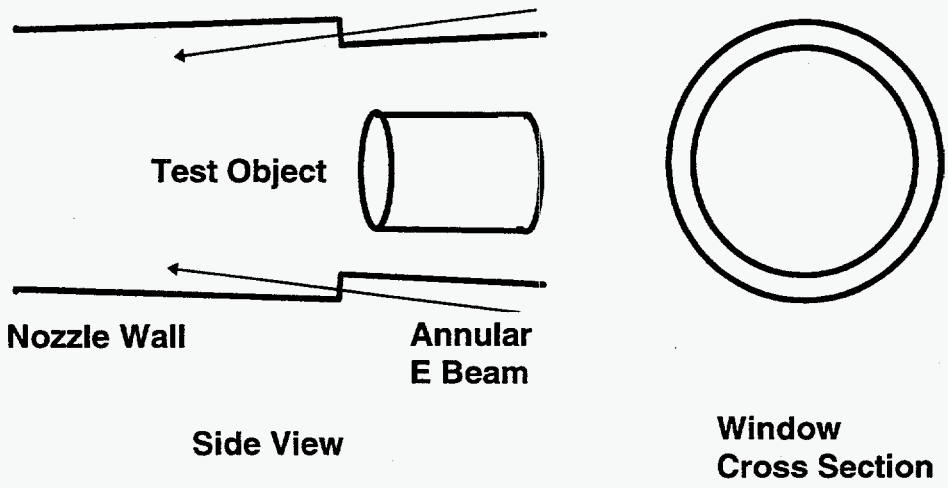

Figure 4.2. Configuration for axial electron beam with annular entrance window.

Table 4.2 shows typical heating conditions for an annular configurations. The heating rate is much reduced and the window material can survive the required 0.1 seconds.

However, even longer times may be achievable. Thermal radiation will remove heat fairly effectively if the foil is thin enough that the total heat source is manageable. The surface heat flux (q_b) to each side of a foil resulting from beam heating is

$$q_b = \frac{SIw_f}{2A} \qquad (4.3)$$

The heat flux removed by thermal radiation from each side is

$$q_r = \varepsilon\sigma\left(T_s^4 - T_b^4\right) \qquad (4.4)$$

Table 4.2. Typical heating conditions for an annular e-beam window.

Beam Size	3.0 m diam x 0.2 m thick
Beam Area	19000 cm^2
Current	100 A
Wall Heating Rate (Carbon)	13.3 °/ms
Time to "Melt"	0.27 sec

where ε is the foil emissivity, $\sigma = 5.67 \times 10^{-8}$ W/m^2 K^4, T_s is the foil surface temperature, and T_b is the temperature of the background surrounding material. If graphite is used and if the emissivity is about 0.9, and if the background temperature is negligible, then the radiant heat flux will equal the heat generated by the beam when the surface temperature is 3657 K. (A thinner foil would yield a lower steady temperature.)

The steady-state temperature rise within the foil is:

$$\Delta T = \frac{q_b \Delta x}{4k} \tag{4.5}$$

where Δx is the foil thickness and k is the foil thermal conductivity. For the graphite foil, this is 130 K. Adding this to the surface temperature results in 3787 K, which is below the sublimation temperature of 3925 K. Thus it is possible that a graphite window could survive well beyond 0.28 seconds (although a thinner foil would give more margin for safety). These results are summarized in Table 4.3.

Table 4.3. Beam heating in annular entrance windows.

Inputs:			
Electron beam:			
voltage (MV)	5	5	5
current (A)	90	85	90
inner radius (m)	1.47	1.47	1.47
outer radius (m)	1.67	1.67	1.67
deposition density (W-m^2/kg-A)	200000	200000	200000
E-beam window:			
material	graphite	molyb-denum	amorphous diamond
density (kg/m^3)	2000	10200	3100
thickness (m)	0.001	0.0001	0.0004
thermal conductivity (W/m K)	35	138	100
emissivity	0.9	0.9	0.9
heat capacity (J/kg K)	711	247	711
melting temperature (K)	3925	2983	3925
Outputs:			
Beam area (m^2)	1.97	1.97	1.97
Foil heat-up rate (K/s)	12832	34885	12832
Time to melt without cooling (s)	0.28	0.08	0.28
Steady foil heat flux to each side (MW/m^2)	9.12	4.39	5.66
Foil surface temp. to remove flux (K)	3657	3046	3245
Foil internal delta-T to remove flux (K)	130	2	11

Columns 3 and 4 of Table 4.3 give additional possible window configurations. Molybdenum is a high-temperature metal that would be a good candidate if it could be made thin enough. Amorphous diamond is another possible window material (although somewhat exotic at present). It is black with a high emissivity, and has a very high thermal conductivity. It is currently only available in small-area samples (1 cm^2).

4.3 Axial Beam with Beam Injection through a Small Open Window

Another approach to injecting the beam into the nozzle without excessive heating of the nozzle wall is to eliminate the physical window between the wind-tunnel nozzle and the accelerator entirely. Instead, there would be a long, skinny, slightly curved tube which the beam would follow. Strong pumping and cryogenically-cooled panels would be used to stop the flow of air back toward the accelerator. This technique is called differential pumping. This approach would be feasible if done at the down-stream end of the nozzle where the air pressure is very low. Figure 4.3 shows a potential configuration.

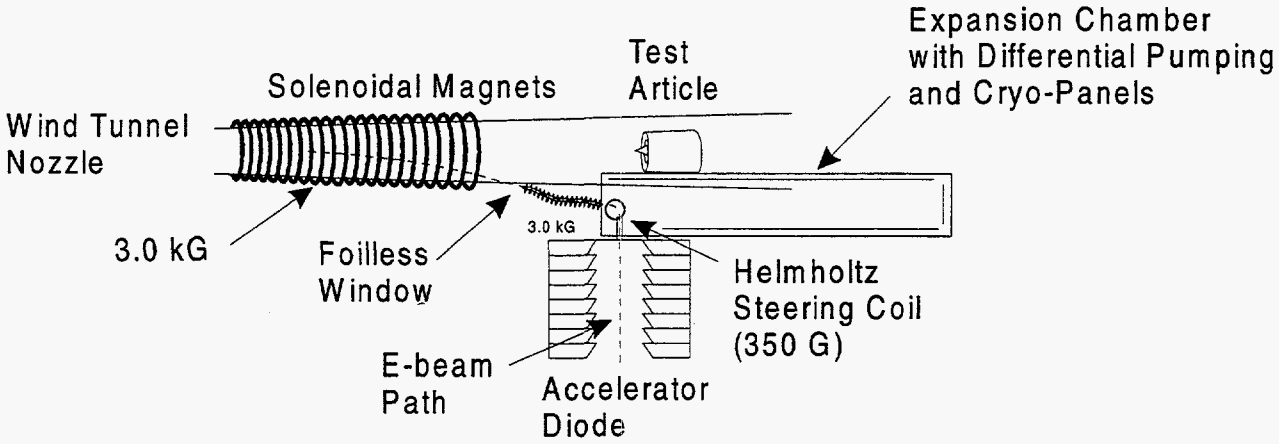

Figure 4.3. Beam injection through a small open entrance window.

The advantages of this approach are (1) easier and less-costly construction of the accelerator, (2) no generation of plasma on the entrance window which could flow back to the accelerator diode and short it out, (3) no maintenance or replacement required for the entrance window, and (4) the potential for very long run times, if the differential pumping can be maintained.

5. Magnetic Guiding of Electron Beams

If the electron beam is injected at the downstream end of the wind tunnel nozzle, it must be guided the full length of the nozzle and focused into the tight section where the high-density

gas is to be heated. Focusing and propagation of electron beams has been studied extensively by the accelerator community, by the Navy, and by the Strategic Defense Initiative Office. The Navy research concentrated on high-current (>10 kA) beams propagating in full density air. SDIO concentrated on 1-kA beams in <1-mTorr air. Some exploration was made in the intermediate pressures. Lawrence Livermore National Laboratory, Sandia National Laboratories, Naval Research Lab, Naval Surface Warfare Center, and Mission Research Laboratory (Albuquerque) were the primary institutes involved in this area. Numerous codes and much experimental expertise were developed.

The high beam currents and short rise times (100 ns) used in those programs gave rise to various space-charge problems and instabilities that are not likely to be of concern here because of the lower current and very long rise time. These instabilities include resistive hose, ion hose, filamentation, two-stream, and wakefield. In addition, use of an applied axial magnetic field should stabilize the beam while guiding it down the tube. The defense missions could not use magnetic guiding because the applications were all in free space.

Under the SDIO program, Sandia propagated a 1-kA, 2.5-MeV electron beam 90 meters through a thin gas (30 microTorr) by using a laser-generated plasma channel to guide it.[4] They used a solenoidal magnet to focus the beam from a 6-cm radius at the accelerator down to a 3-cm radius. The space charge of the beam stopped the beam convergence at 3 cm, at which time the plasma channel picked up the beam and guided it down the tube. The beam diameter at 90 m was still 3 cm. The team also used a 30-G axial field to guide 400-V electrons along the centerline of a 21-m tube (in order to make a plasma channel before the laser became operational). In this case the 2.5-MeV beam was first guided for 2 m on a thin wire and then was picked up by the plasma channel. These are just a few of the techniques that can be applied to guiding electron beams down tubes.

The approach for guiding the electron beam in the wind tunnel is to inject it at a shallow angle into the low-pressure end of the nozzle. The injection angle should be low to minimize beam emittance when it turns at the axial centerline. At the point where the beam reaches the axial centerline, a long axial magnetic field will begin which will capture the beam and conduct it down the tube. The test object will be in the fringe of the magnetic field. Heating of the nozzle air will be negligible until the beam gets close to the nozzle throat where the air is dense. At that point, the field will converge and strengthen and will bring the beam in with it. With proper field design, the beam will fill most of the nozzle in this region where the air is dense and most of the energy deposition occurs.

An estimate of the required field strength can be obtained from the formula for the Larmor radius. The Larmor radius for a relativistic electron is the radius of the circular or helical path that an electron follows as it travels around or along a magnetic field line. The formula is:

$$r_L = \frac{V\beta_p}{cB}\sqrt{\frac{\gamma+1}{\gamma-1}} \qquad (5.1)$$

where V is the electron energy in electron volts, β_p is the perpendicular component of the velocity, c is the speed of light, B is the magnetic field, and γ is the relativistic mass fraction:

$$\gamma = \frac{V}{0.511\,\mathrm{MV}} + 1 \qquad (5.2)$$

For example, where the beam is first injected into the nozzle, β_p would be low. If the beam voltage is 5 MV and if $\beta_p = 0.1$, then a field of 1 kG (0.1 T) would yield a 1.8-cm Larmor radius. If these field lines are then compressed down by a factor of ten in diameter, the field strength would increase by a factor of 100 (to 100 kG). If β_p also increases due to scattering in the air as the beam travels, then the new Larmor radius would be about 0.16 cm (for $\beta_p = 0.9$). The actual beam radius will be larger than the Larmor radius depending on the initial beam injection radius and the amount of scattering during transport. Beam optics and scattering codes will be run to better determine the magnetic field configuration needed and the resulting beam radius.

6. Large-Scale Wind Tunnel with E-Beam Heating

Figure 6.1 shows the configuration for a large-scale wind tunnel heated by an axial beam. The entrance of the e-beam into the wind tunnel is through a small-diameter port. This port is just upstream of the article to be tested. Because the flow is hypersonic, the small flow disturbance caused by this port will remain close to the wall for a long time and will not impact the test article.

The beam is injected at a shallow angle and slowly spirals toward the center of the nozzle. As it propagates toward the nozzle throat, it becomes azimuthally uniform due to the energy spread among the individual electrons. (This is a common effect seen in all electron beams.) The gas density is very low for most of this trip, so there is negligible beam absorption or gas heating until the beam reaches the small-diameter portion of the nozzle near the throat.

The accelerator is long-pulse electrostatic accelerator which uses a Marx generator for the voltage source. The Marx generator consist of a set of large capacitors which are charged in parallel to around 50 kV, and then quickly switched to a series configuration adding up to 5 or 10 MeV. It is the basis of many electrostatic accelerators throughout the DoD and DOE labs.

The high voltage is held off in the diode by a long, large-diameter stack of insulating rings. This stack must be cantilevered if it is horizontal; an example of this is the 1-m long stack in the Troll accelerator at Sandia (demonstrated at 4 MeV for 1 microsecond). However, we will want to hold off the voltage for very long times and possibly go to higher voltages than 5 MeV, so the recommended configuration is vertical, which does not require a cantilever. This is the approach typically used in Van de Graaff generators which support 10 to 20 MeV indefinitely (hours). Because of this vertical configuration, the accelerator will extend either above or below the wind-tunnel nozzle.

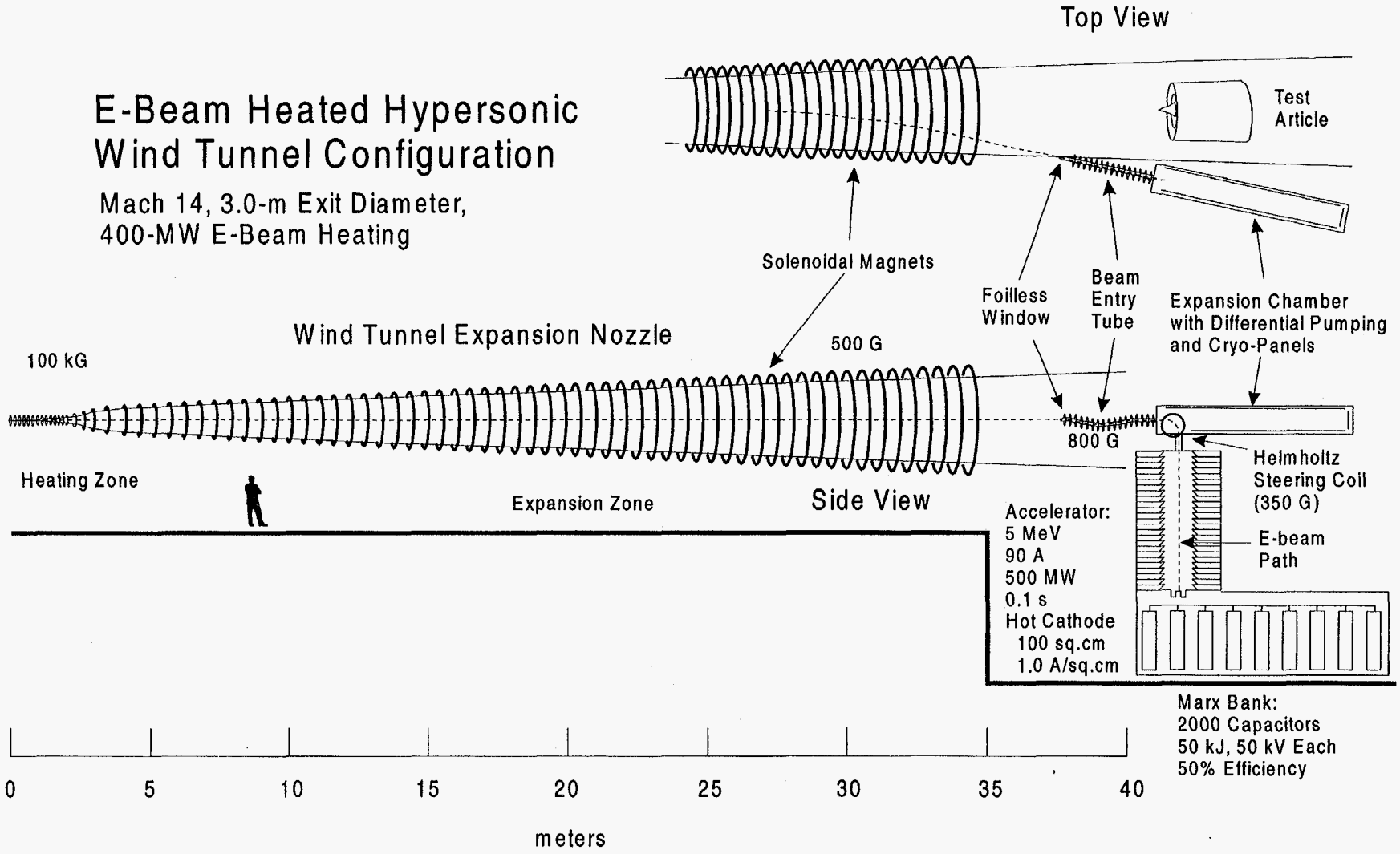

Figure 6.1. Large-scale wind-tunnel configuration with e-beam heating.

Figure 6.2 shows an example of an electrostatic accelerator which is similar in design to the one proposed. It is the "Troll" accelerator at Sandia National Laboratories and produces about 1000 A at 4 MeV for 1 microsecond; [5] the proposed wind-tunnel accelerator is 90 A at 5 MeV for 0.1 seconds. The main difference will be in the size of the capacitor bank to drive the long-duration current (although in the Troll accelerator about 90% of the stored energy is not utilized).

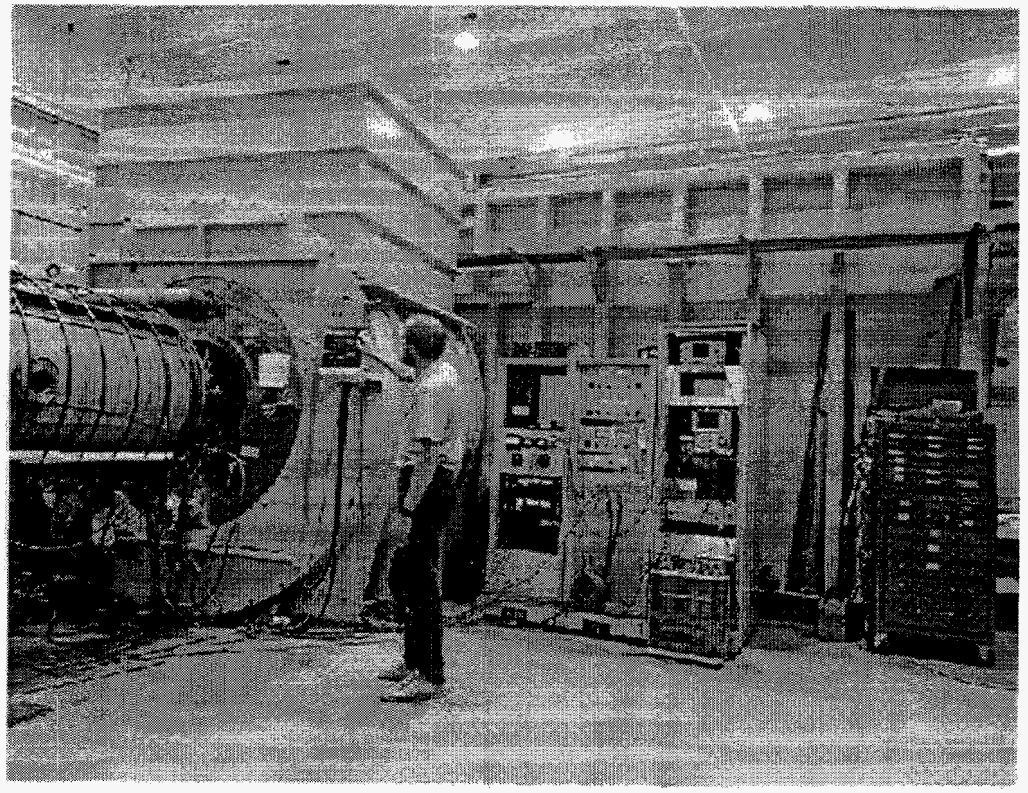

Figure 6.2 Troll accelerator (1000 A, 4 MeV, 1 microsecond).

Figure 6.3 shows an example of a small beam-propagation tube (2 m long) similar to the proposed isolation tube between the accelerator and the wind tunnel. It is wrapped with wire to produce 800 G, which is similar to the proposed 500 G for the wind tunnel. This tube transported a 1900-A, 2.5-MeV electron beam from the Troll accelerator while maintaining the beam diameter at about 4 cm.

Figure 6.4 shows an example of a large-diameter steel tank (0.91-m diameter) with a coarse solenoid around it, similar to the one needed for the wind tunnel. This solenoid produced only 60 G, but it could be modified to produce the desired 500 G with a higher-voltage power supply to drive it.

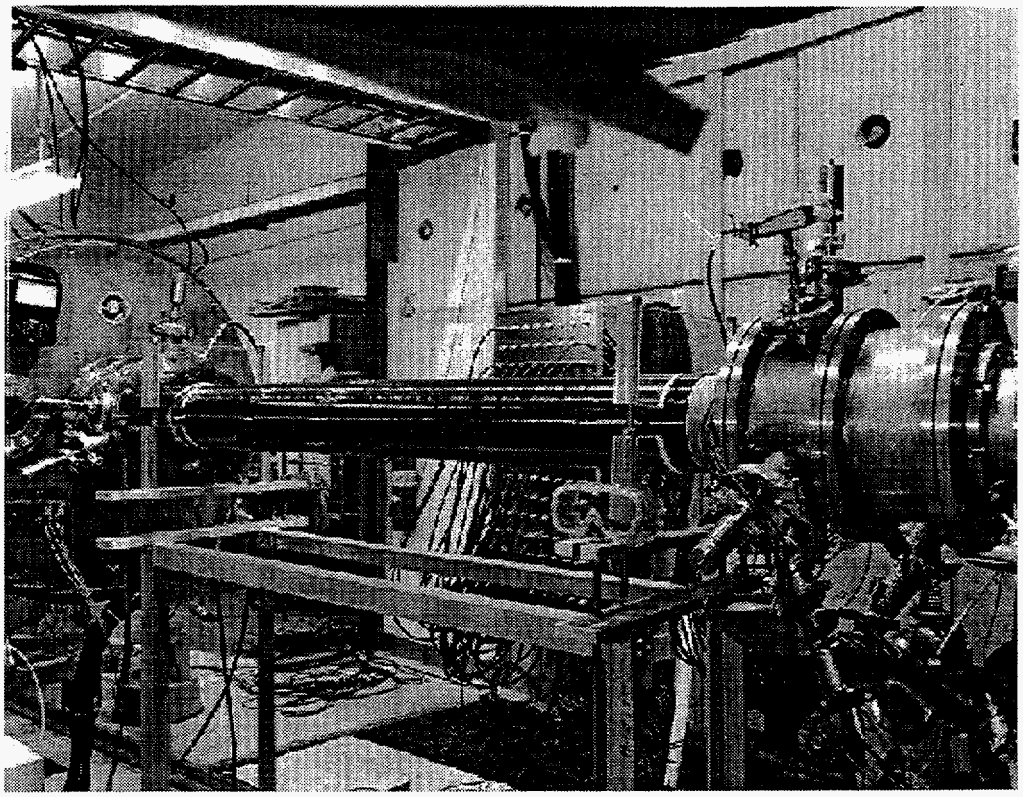

Figure 6.3 E-beam drift tube with 600-G solenoid wrapped around it.

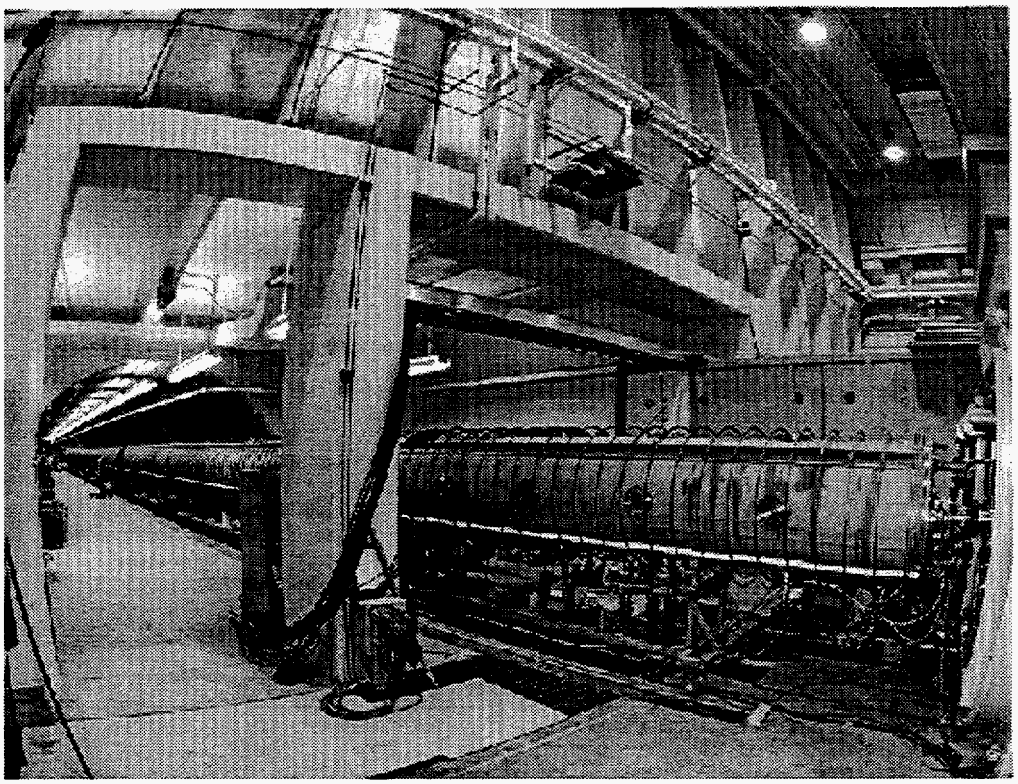

Figure 6.4 Long vacuum tank with coarse 60-G solenoid wrapped around it.

Figure 6.5 shows a set of 35 solenoidal magnets at Sandia National Laboratories with an inner diameter of 5 cm. The first 30 magnets have been demonstrated at 100 kG and the last 5 have been demonstrated at 240 kG (for about 0.15 ms).[6] Magnets similar to these would be needed for the small-diameter section of the wind tunnel nozzle near the throat.

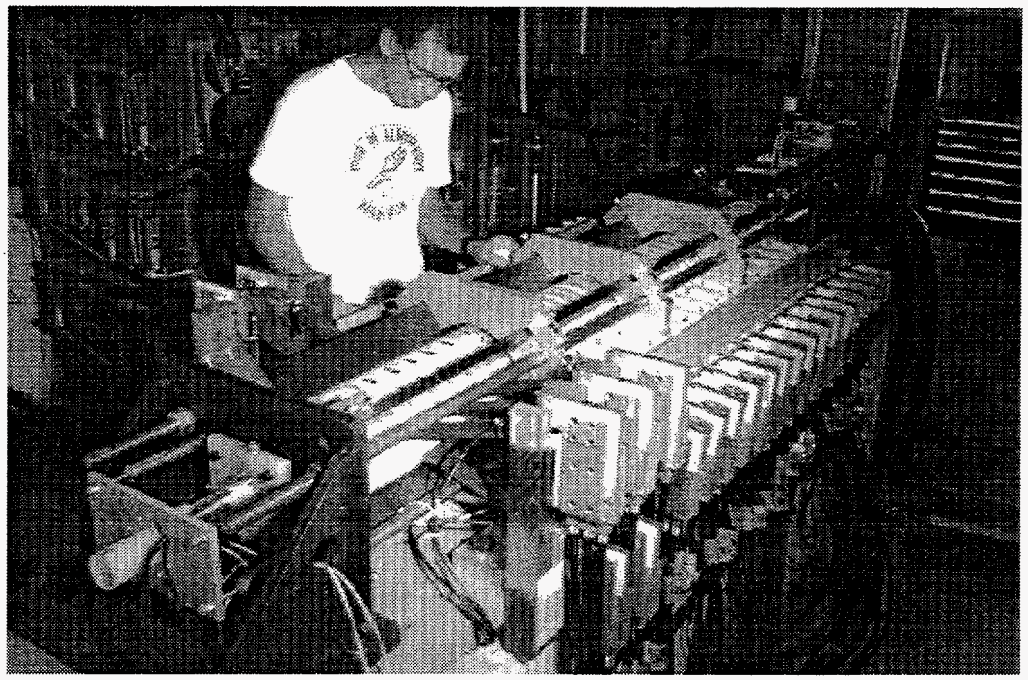

Figure 6.5 Line of solenoidal magnets (30 at 100 kG, 5 at 240 kG).

Table 6.1 shows the point-design parameters for the wind tunnel. The details of the expansion nozzle are not precise because we have not yet made a self-consistent computer simulation of e-beam heated gas expansion, and so we are using the configuration generated for laser-beam heated expansion. But the differences should be inconsequential and easily incorporated into a revised design later.

Table 6.1. List of parameters for a large-scale hypersonic wind tunnel.

Gas exit velocity	Mach 14
Nozzle exit diameter	2.8 m
Nozzle inlet diameter	0.80 cm
Energy deposited by e-beam (MW)	400 MW
Duration	0.1 s
Accelerator high-voltage source	Marx Generator
Output voltage	5 MeV
Number of capacitors	2000
Energy per capacitor	50 kJ
Total stored energy	100 MJ
Beam generation efficiency	50%
Pulse shaping	Guilleman Circuit
Input voltage per capacitor	50 kV
Accelerator type	Electrostatic (Diode)
Insulator stack length	5 m
Insulator stack outer diameter	<3 m
Cathode type	Hot emission
Cathode emission area	100 cm^2
Total current	90 A
Emission current density	1.0 A/cm^2
Beam injection system	Foilless window with differential pumping
Pressure in wind-tunnel nozzle	0.76 Torr
Pressure in accelerator diode	10^{-6} Torr
Entrance window diameter	5 cm
Differential pumping technique	pipe bends, cooled walls, expansion chamber, pumps
Beam guidance technique	Axial magnetic field
In entrance tube	
Magnetic field strength	800 G
Beam transverse/forward vel.	0.05
Beam diameter	2.3 cm
Near exit of wind-tunnel nozzle	
Magnetic field strength	500 G
Beam transverse/forward vel.	0.1
Beam diameter	7 cm
Near throat of wind-tunnel nozzle	
Magnetic field strength	100 kG
Beam transverse/forward vel.	.9
Beam diameter after scattering	1.0 cm

The expansion nozzle and gas conditions for this design is the same as used in Case 1 of reference 1. The overall conditions for this case are summarized in Table 6.2. The initial temperature in the entrance gas plenum is chosen to be low enough to avoid formation of NO and NO_2, and the pressure is chosen to be reasonably achievable. However, in order to obtain the desired outlet gas conditions (Mach 14 and 190 K at 0.00150 atm, for this case), 400 MW must be deposited in the flow stream just after the throat.

Table 6.3 and Figure 6.6 give the conditions in the wind tunnel, as obtained from Ref. 1. The nozzle radius changes strongly between 0.3 and 2.3 m. This induces a strong change in pressure and density. The axial areal density in Figure 6.6 is the integration of gas density starting at the nozzle exit and heading toward the throat. It is a good measure of how far the electron beam will penetrate.

Note that the laser energy is added primarily from axial locations 0.15 to 1.2 m. Unfortunately, the e-beam energy is added primarily in the region from 0.55 to 1.0 m, so the match of energy deposition to beam expansion is not correct. We need to develop a better-matched nozzle expansion profile to have a truly self-consistent design. But the dominant features of beam guiding and heating in dense gas will be very similar to what is described here using the Reference 1 design.

Table 6.2. Conditions for the baseline wind tunnel (Case 1 of Ref. 1.)

Stagnation (Plenum) Conditions	
Temperature	900 K
Pressure	25,100 atm
Density	1260 kg/m^2
Enthalpy	2.77 MJ/kg
Entropy	4900 J/kg-K
Flow Rate	79.0 kg/s
Throat Conditions at Mach 1	
Velocity	1800 m/s
Temperature	610 K
Density	932 kg/m^3
Diameter	0.774 cm
Pressure	7260 atm
Exit Conditions	
Mach #	14.3
Velocity	3800 m/s
Temperature	190 K
Density	0.0028 kg/m^3
Diameter	2.8 m
Pressure	0.00150 atm

Table 6.3. Wind tunnel conditions for 400-MW of energy addition, Case 1, Ref. 1. z is axial distance from the Mach-2.0 location, r is wind-tunnel inner radius, P is pressure, T is temperature, Axial Sum is the integration of density over distance starting from the downstream end of the wind tunnel, and PwrDep is the power deposited by the laser.

z	r	P	T	Density	AxialSum	Pwr Dep
(m)	(m)	(atm)	(K)	(kg/m^3)	(kg/m^2)	(MW/m)
0.0	0.0040	2000	500	1419.6000	415.9194	0
0.1	0.0045	2000	600	1183.0000	285.7894	100
0.2	0.0050	2000	900	788.6667	187.2061	315
0.3	0.0055	2000	1300	546.0000	120.4727	375
0.4	0.0060	2000	1650	430.1818	71.6637	390
0.5	0.0065	1600	2000	283.9200	35.9586	415
0.6	0.0080	600	2000	106.4700	16.4391	470
0.7	0.0150	150	2000	26.6175	9.7847	480
0.8	0.0225	80	2000	14.1960	7.7440	435
0.9	0.0300	75	2200	12.0989	6.4293	310
1.0	0.0325	65	2400	9.6119	5.3437	250
1.1	0.0360	60	2400	8.8725	4.4195	20
1.2	0.0380	50	2300	7.7152	3.5901	0
1.3	0.0415	40	2200	6.4527	2.8817	
1.4	0.0450	30	2100	5.0700	2.3056	
1.5	0.0500	21	1990	3.7452	1.8648	
1.6	0.0560	16	1880	3.0204	1.5266	
1.7	0.0620	12	1770	2.4061	1.2552	
1.8	0.0690	8	1660	1.7104	1.0494	
1.9	0.0770	6	1550	1.3738	0.8952	
2.0	0.0900	4	1440	0.9858	0.7772	
2.5	0.1600	0.7	820	0.3030	0.4550	
3.0	0.3000	0.1	550	0.0645	0.3631	
4.0	0.4200	0.07	445	0.0558	0.3030	
6.0	0.5000	0.03	390	0.0273	0.2198	
8.0	0.6000	0.018	340	0.0188	0.1738	
10.0	0.6800	0.01	300	0.0118	0.1431	
15.0	0.8800	0.006	265	0.0080	0.0935	
20.0	1.0700	0.003	240	0.0044	0.0623	
30.0	1.4000	0.0015	190	0.0028	0.0261	

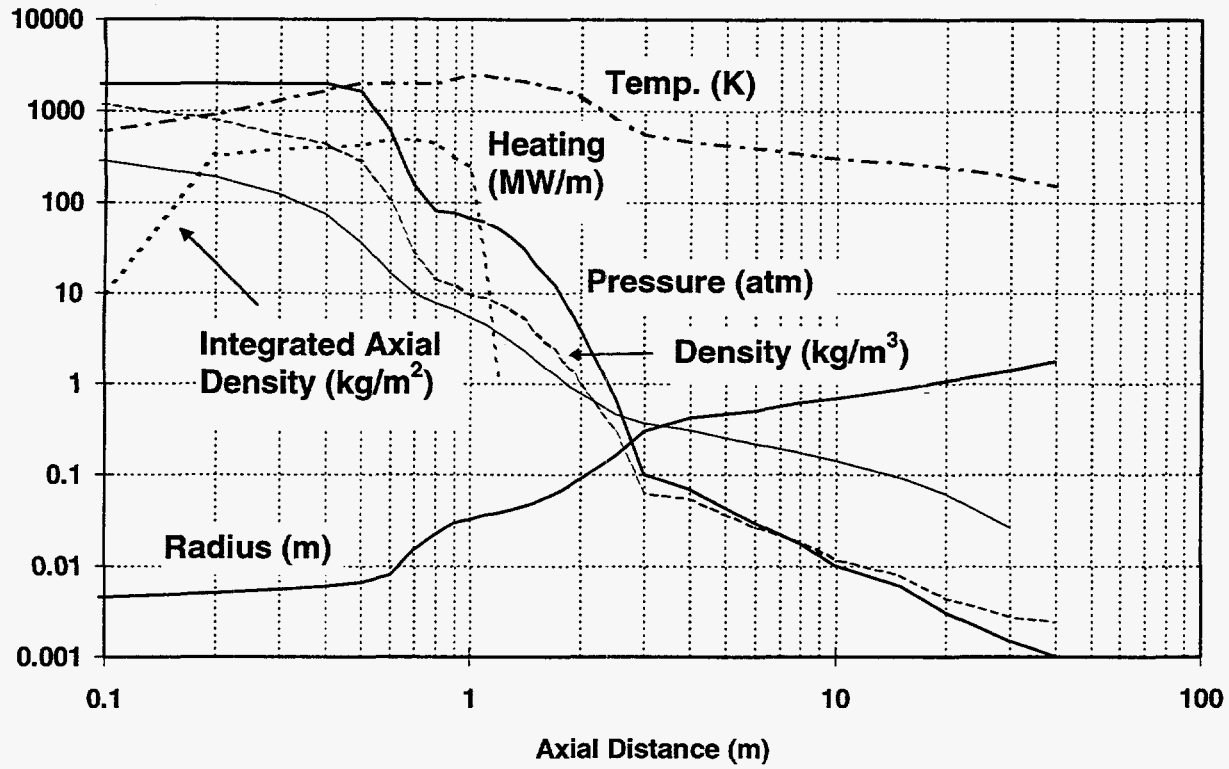

Figure 6.6. Wind tunnel baseline conditions.

Figures 6.7 shows the nozzle profile in true aspect ratio and Figure 6.8 shows a close-up of the heated region. Note how small the heated zone is compared to the rest of the nozzle. This presents a challenge to beam transport and focusing.

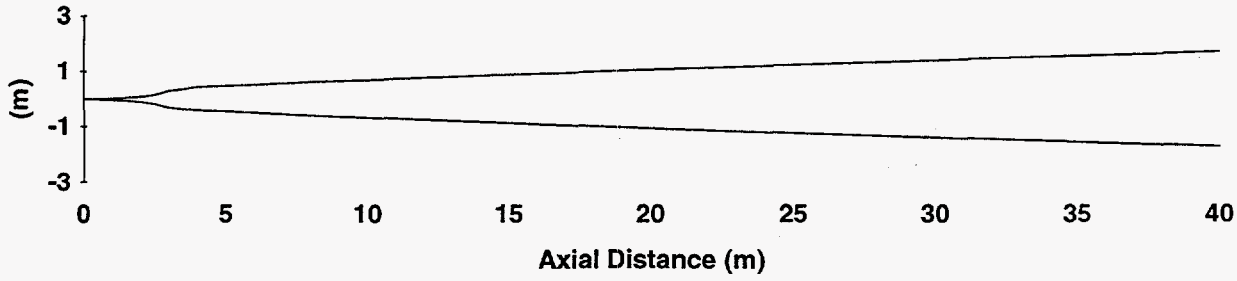

Figure 6.7. Large-scale wind tunnel nozzle profile.

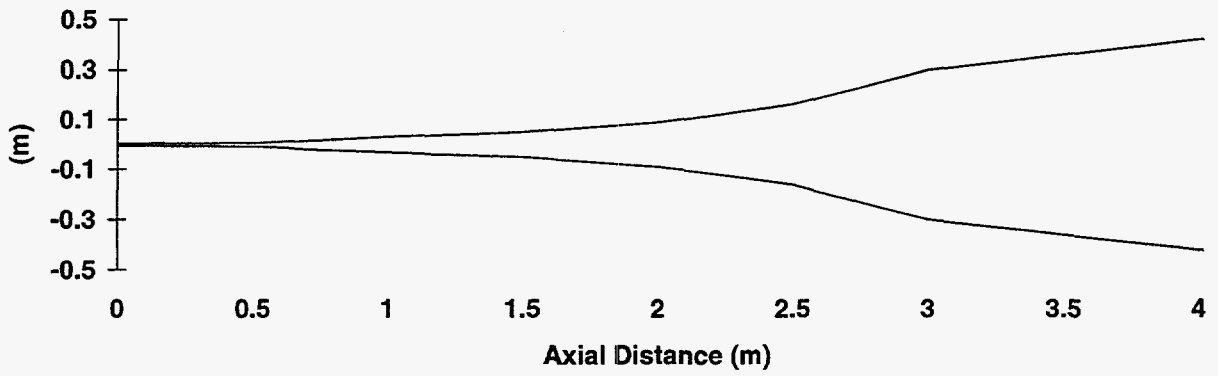

Figure 6.8. Large-scale wind tunnel nozzle profile near the heated region (0.1 to 1.1 m)

We completed a computer simulation of the electron beam being guided by the magnetic field and depositing energy in the high-density air at the start of the expansion nozzle of the large-scale wind tunnel. The code used was CYLTRAN, which is part of the ITS suite used by Sandia and the DoD community for determining radiation dosage in various targets from electron beams and gamma rays. It has had extensive development and benchmarking under Department of Energy and Defense Nuclear Agency (currently DSWA) programs. The CYLTRAN code is a Monte-Carlo code which follows individual primary electrons and a sampling of the numerous cascade-shower electrons. The intent of this simulation is to determine whether the beam is adequately guided by the applied magnetic field in the nozzle, and to determine where the energy is deposited.

Figure 6.9 shows the modeling conditions for the zones at the start of the expansion region of the wind tunnel (not to scale). A 5-MeV, 90-A, 450-MW (to allow for some losses) electron beam is injected up the nozzle from the downstream end. The e beam enters the modeling region with a 2.8-cm radius, uniform distribution, and zero transverse temperature. (Scattering will increase its temperature very rapidly once the simulation begins, so the initial beam temperature is not important.) The applied magnetic field at this region increases from 2.3 kG to 100 kG as the field lines converge toward the throat. (A 100 kG solenoidal field is challenging to make but readily achievable with present technology, as will be described in a later section.) The equation for the magnetic field is:

$$B = (100\ \text{kG})\left(\frac{26.4\ \text{cm}}{z\ -\ 26.4\ \text{cm}}\right)^2 \qquad (6.1)$$

The simulation involved the modeling of the specific trajectories of 200,000 source electrons. Figure 6.10 shows the trajectories of a few individual electrons for the case with no air in the wind tunnel. This demonstrates how the field guides the beam when there is no air to scatter

the electrons. Figure 6.11 shows electron trajectories for the case where there is air present in the nozzle in the conditions shown in Figure 6.10. The figure is drawn to proper scale. Figure 6.12 shows the same result but expanded vertically for better clarity.

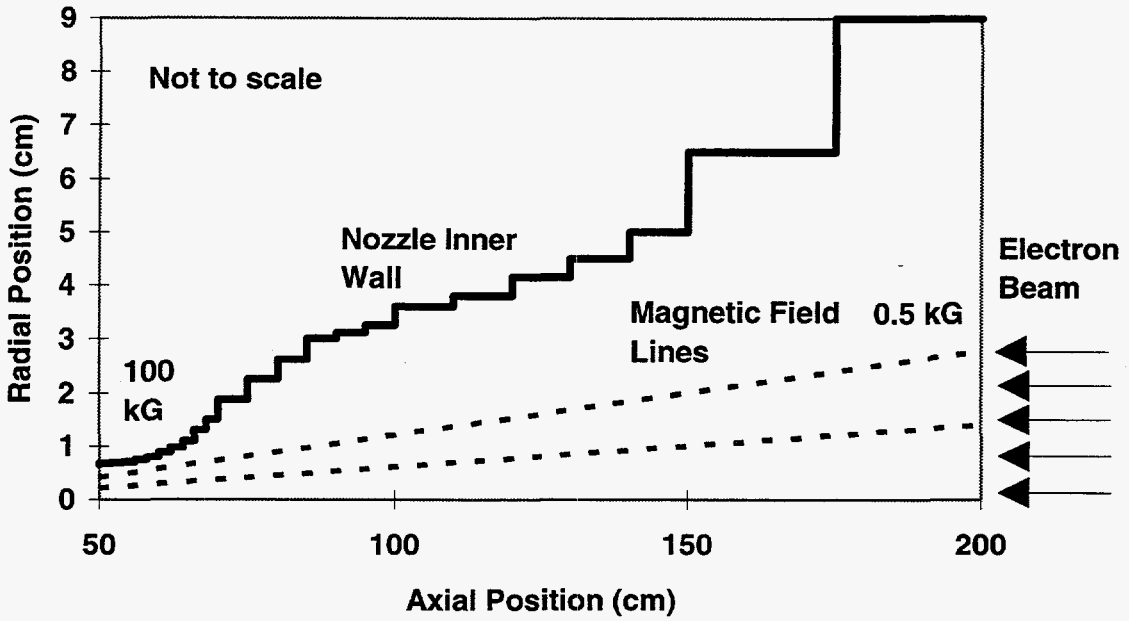

Figure 6.9. Geometry for CYLTRAN model of electron beam (not to scale)

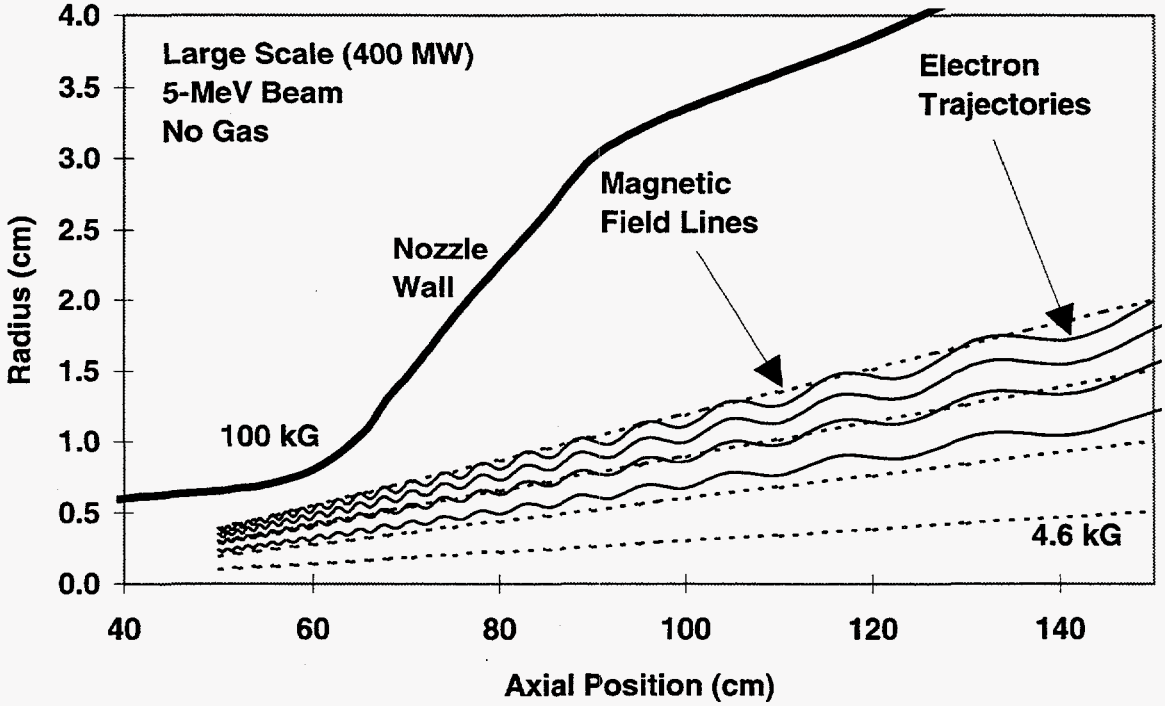

Figure 6.10. Electron beam with no gas present. (Not to scale.)

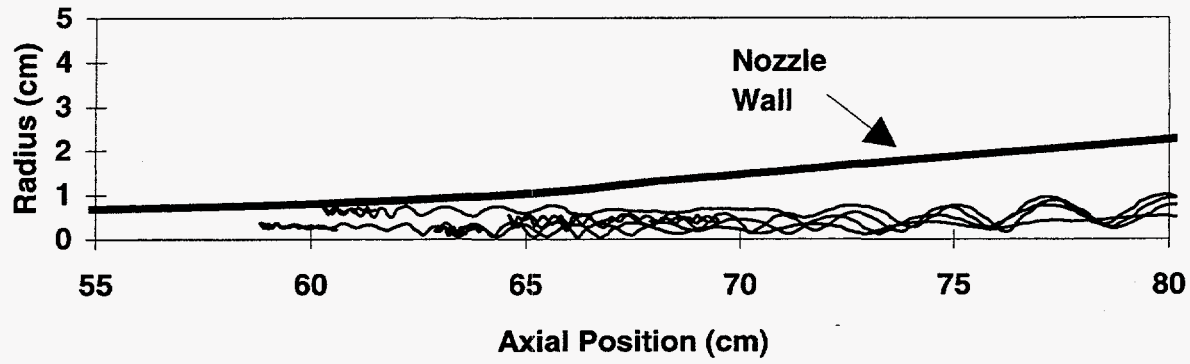

Figure 6.11. Electron trajectories for the case where there is air present in the nozzle in the conditions shown in Figure 6.6. 200,000 electron trajectories were calculated, but only four are shown. The figure is drawn to scale.

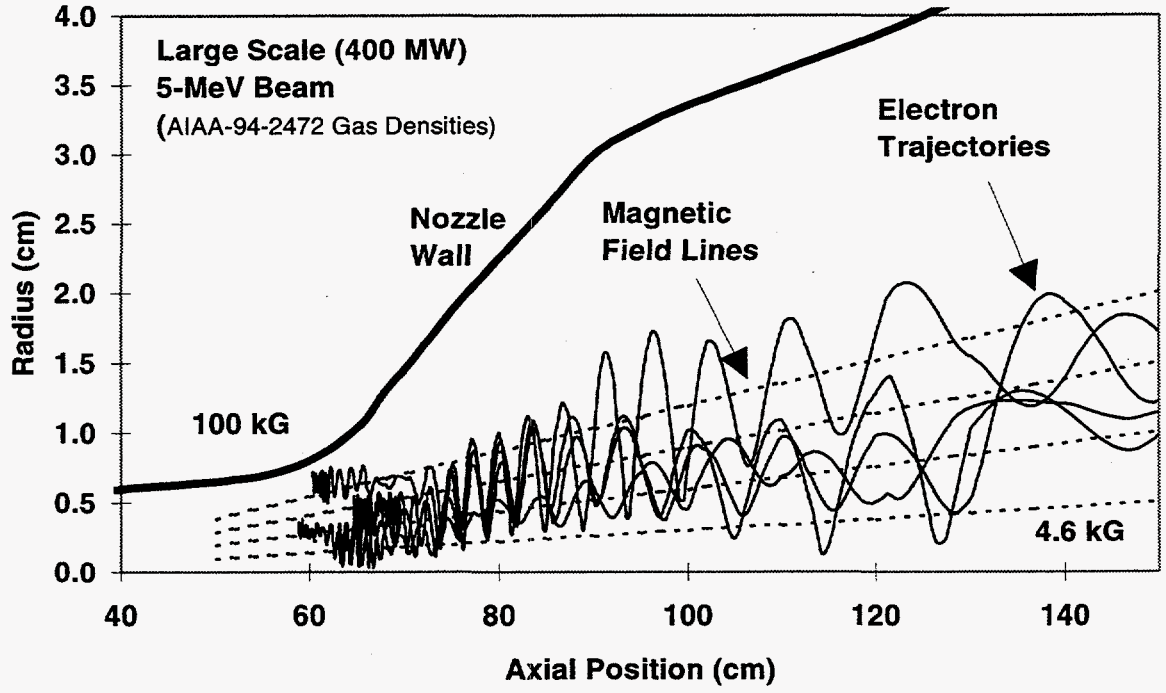

Figure 6.12 Same as Figure 6.11 but expanded in the vertical direction for better clarity.

Figure 6.13 shows an expanded view of the zone from 50 to 75 cm with ten sample electrons instead of four. Scattering greatly randomizes the beam propagation, but the applied magnetic field confines the beam and guides it toward the nozzle throat while keeping it away from the walls. Most of the electrons run out of energy before reaching the 60-cm location.

Some are reflected back, and a small percentage strike the wall (one is shown). The electrons continuously deposit energy into the gas as they travel, thus heating the air in situ.

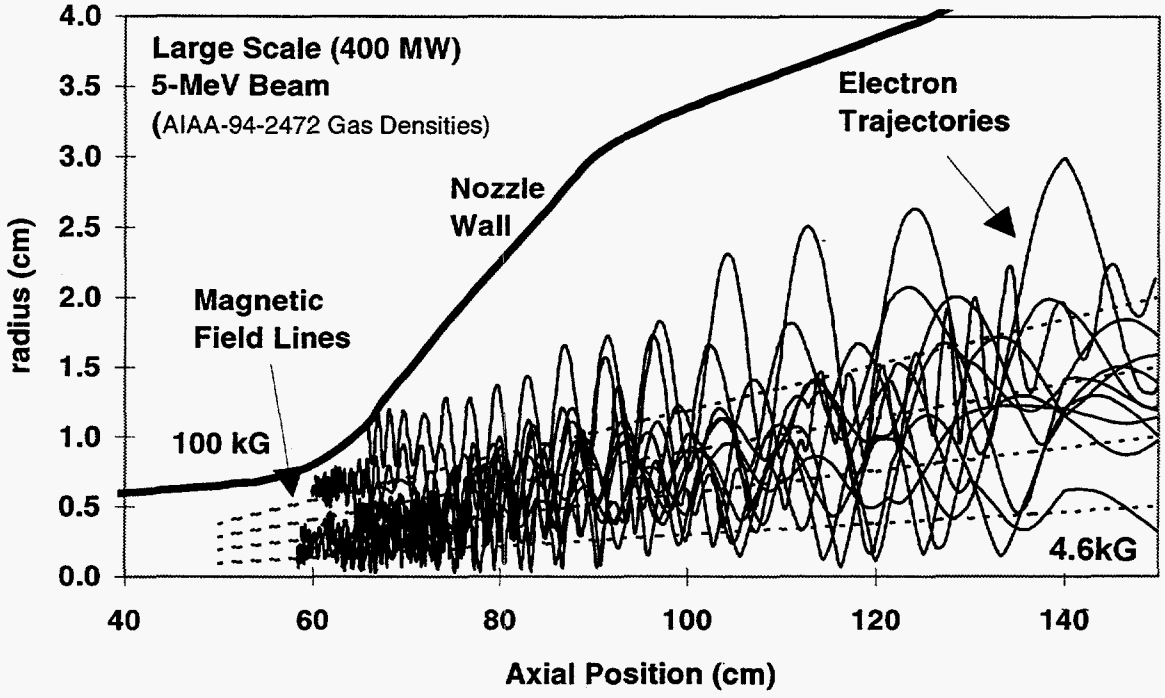

Figure 6.13 Simulation results for ten sample electron trajectories, again expanded vertically for better clarity.

Figure 6.14 shows the axial-profile for various radial locations. Note how the deposition rate per unit mass increases as the beam is compressed toward the throat, but at some point the electrons run out of energy and the deposition goes to zero (near 55 cm). Figure 6.15 shows the radial profile of the energy deposition rate for various axial locations. Note that the width of the energy deposition column decreases with decreasing z to match the convergence of the nozzle. Note also that very little energy is deposited in the nozzle walls.

The e-beam power is deposited in the region from 55 cm to about 100 cm. For comparison, the laser in the Reference-1 case-1 model deposited its energy from about 15 cm to about 120 cm, as displayed in Figure 6.6. To be fully consistent, we need to develop a case in which the wind-tunnel nozzle expands at a rate that matches the energy deposition rate of the e beam. Alternatively, we could mix in some higher-energy electrons to penetrate farther. Nonetheless, these results show that an e-beam could be guided with an axial field in a large-scale wind tunnel, in spite of scattering in the thick wind-tunnel air.

Figure 6.16 shows the beam radius (half width at half maximum) vs. axial location, compared to the nozzle radius. Note that the magnetic field actually compresses the beam as it travels, in spite of scattering in the high-density air. If needed, the field and beam could be

adjusted so that the beam extends closer to the wall, but we would need to be careful of excessive wall heating.

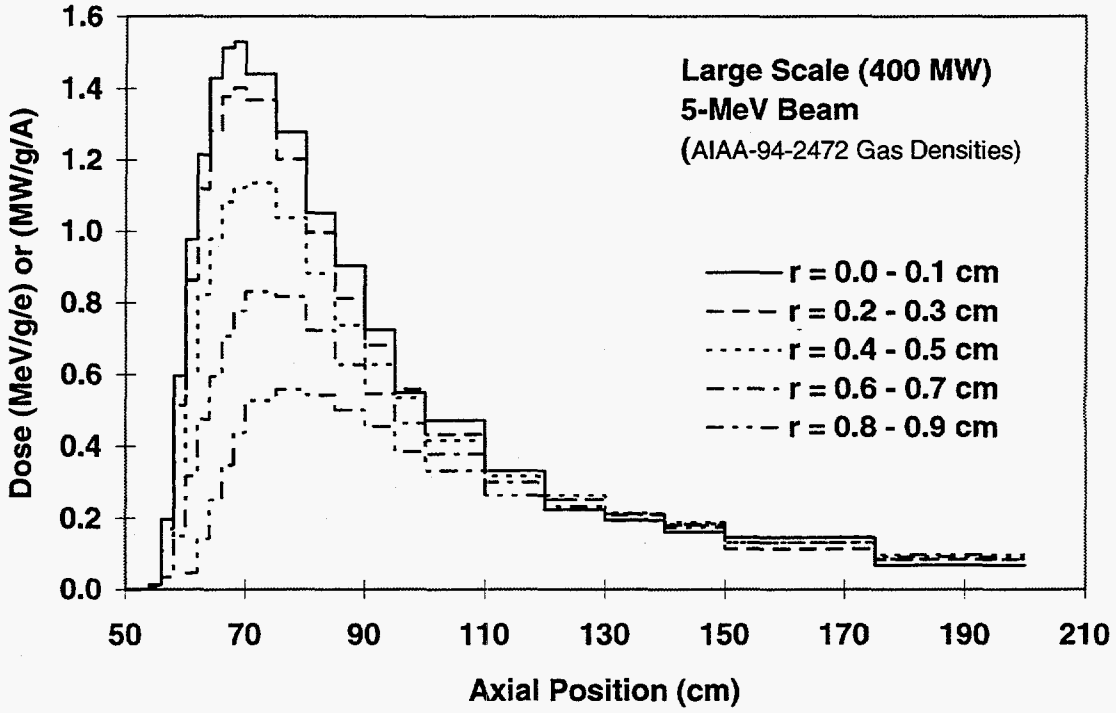

Figure 6.14. Axial profile of the energy deposition rate for various radial locations normalized to the total current in the beam (not local current).

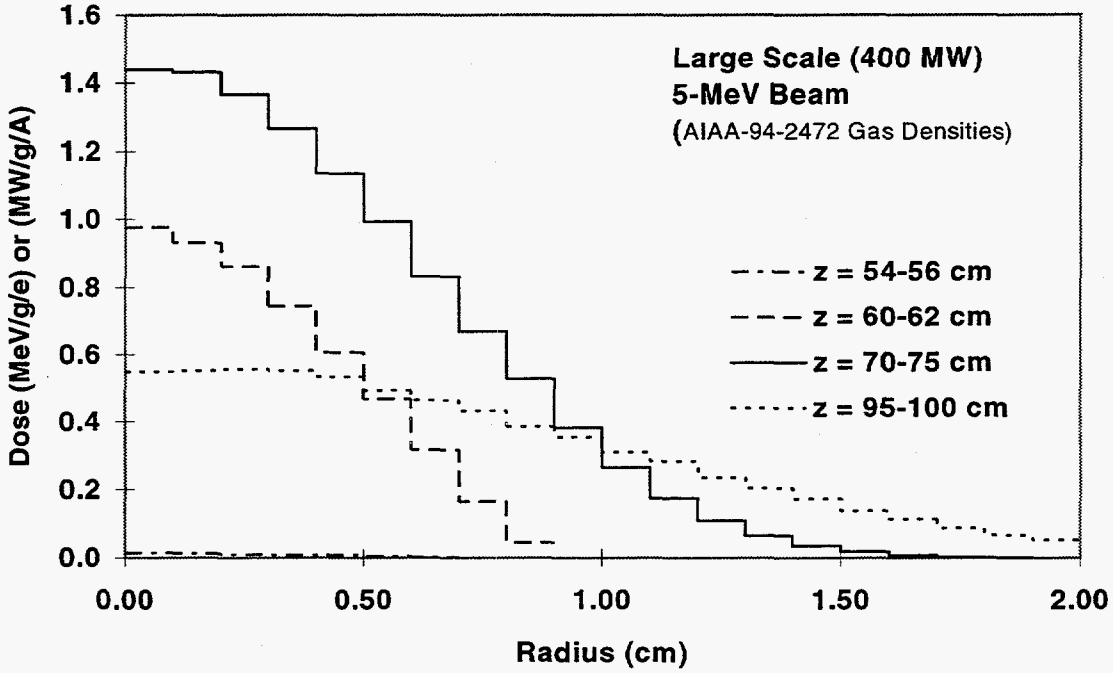

Figure 6.15. Radial-profile for various axial locations.

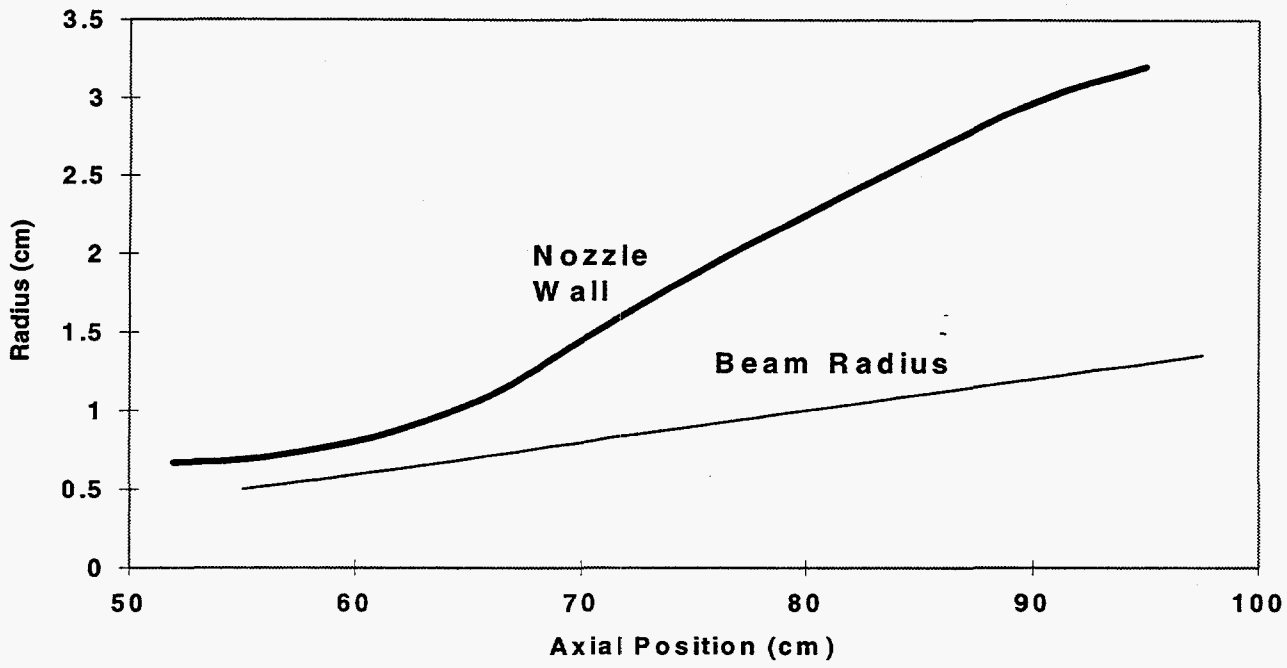

Figure 6.16. Beam radius (at 1/e of maximum) vs. axial position in nozzle.

7. Pilot-Scale Wind Tunnel with E-Beam Heating

Princeton developed a hydrodynamic code to model gas behavior in a wind tunnel heated by an electron beam.[7] With this code they determined a nozzle shape in which the expansion was well-matched to the energy deposition rate from a 21-MW e beam for a pilot-scale wind tunnel with an exit velocity of Mach 12. Figure 7.1 shows the configuration for the pilot-scale design, and Table 7.1 summarizes the key parameters along with those for the large-scale wind tunnel.

The 25-MW e beam delivers about 21 MW into the gas. The baseline design for the accelerator is a single large capacitor bank that discharges for 1.0 second. (An alternative is several small accelerators, each discharging for a fraction of a second and fired in sequence at about a 5 Hz rate.) The beam enters the nozzle region through a small aperture without a foil barrier, so window heating is not a problem. The dimensions and magnetic field strengths have been adjusted to meet the new requirements, but otherwise the geometry is very similar to the large-scale wind tunnel.

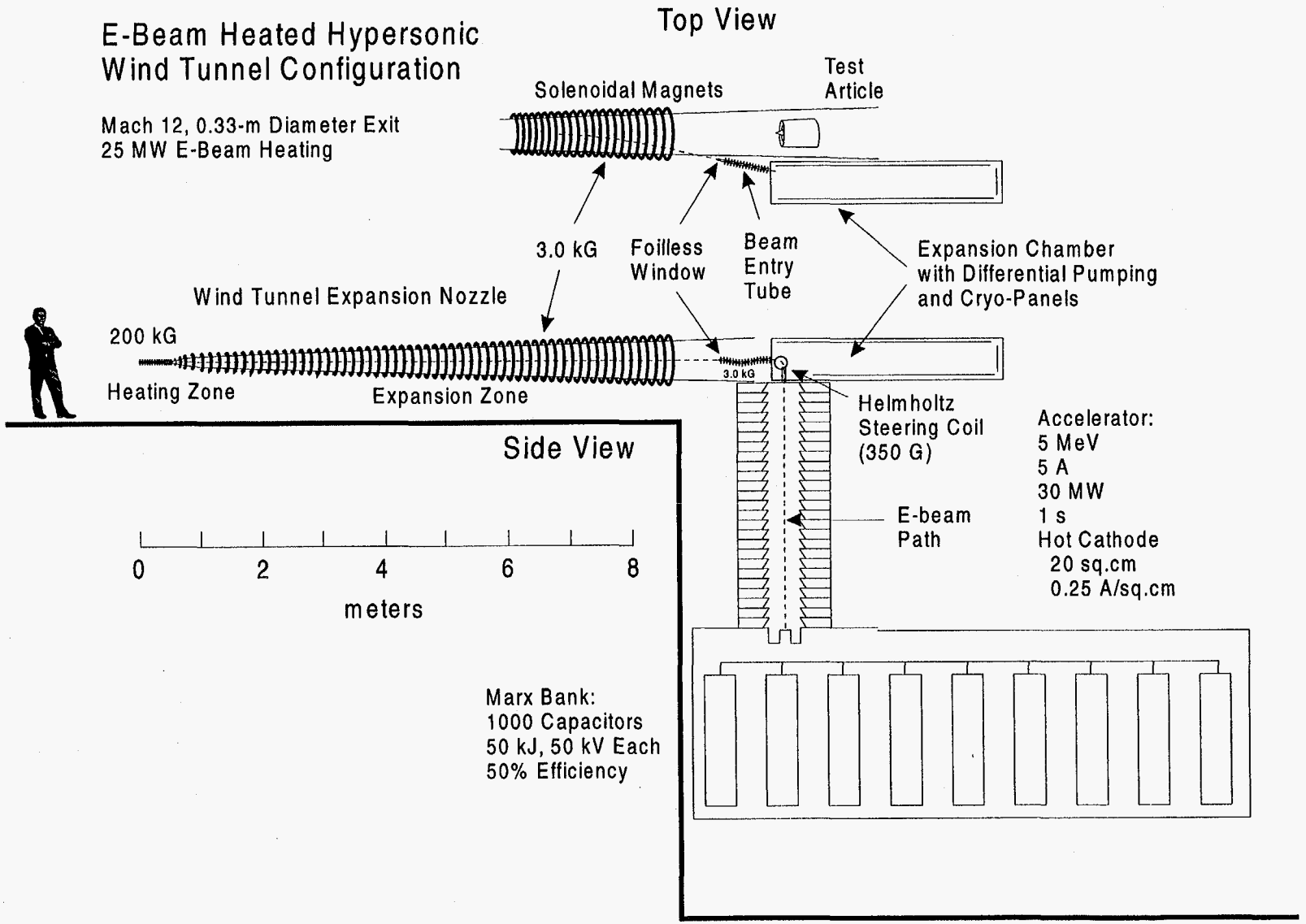

Figure 7.1 Configuration for the e-beam heated pilot-scale wind tunnel.

Table 7.1. List of parameters for the e-beam heating system of a Prototype and a large-scale Radiatively-Driven Hypersonic Wind Tunnel.

System	Pilot-Scale	Large-Scale
Stagnation Conditions:		
Pressure	15,000 atm	25,100 atm
Temperature	1200 K	900 K
Sonic (Throat) Conditions:		
Pressure	5375 atm	7260 atm
Temperature	894 K	610 K
Velocity	1584 m/s	1800 m/s
Exit Conditions:		
Mach Number	Mach 12	Mach 14.3
Pressure	0.0173 atm	0.0015 atm
Temperature	171 K	190 K
Overall Conditions:		
Nozzle inlet diameter	0.30 cm	0.80 cm
Nozzle exit diameter	0.326 m	2.8 m
Nozzle length	8 m	30 m
Mass flow rate	8.3 kg/s	79 kg/s
Duration	1 s	0.1 s
Energy deposited by e-beam (MW)	21 MW	400 MW
E-beam System:		
Accelerator high-voltage source	Marx Generator	Marx Generator
Output voltage	5 MeV	5 MeV
Number of capacitors	1000	2000
Energy per capacitor	50 kJ	50 kJ
Total stored energy	50 MJ	100 MJ
Beam generation efficiency	50%	50%
Pulse shaping	Guilleman Circuit	Guilleman Circuit
Input voltage per capacitor	50 kV	50 kV
Accelerator type	Electrostatic (Diode)	Electrostatic (Diode)
Insulator stack length	5 m	5 m
Insulator stack outer diameter	<3 m	<3 m
Cathode type	Hot emission	Hot emission
Cathode emission area	20 cm^2	100 cm^2
Total current	5 A	100 A
Emission current density	0.25 A/cm^2	1.0 A/cm^2

System	Pilot-Scale	Large-Scale
Beam injection system	Foilless window with differential pumping	Foilless window with differential pumping
Pressure in wind-tunnel nozzle	13 Torr	1 Torr
Pressure in accelerator diode	10^{-6} Torr	10^{-6} Torr
Isolation tube inner diameter	1.2 cm	5 cm
Isolation tube length	3 m	3 m
Isolation tube shape	S-curve, >2-cm offset	S-curve, >10-cm offset
Differential pumping technique	pipe bends, cooled walls, expansion chamber, pumps	pipe bends, cooled walls, expansion chamber, pumps
Beam guidance technique	Axial magnetic field	Axial magnetic field
In isolation tube		
Magnetic field strength	3.0 kG	800 G
Beam transverse/forward vel.	0.05	0.05
Beam diameter	0.61 cm	2.3 cm
Near exit of wind-tunnel nozzle		
Magnetic field strength	3.0 kG	500 G
Beam transverse/forward vel.	0.1	0.1
Beam diameter	1.0 cm	7 cm
Near throat of wind-tunnel nozzle		
Magnetic field strength	200 kG	100 kG
Beam transverse/forward vel.	.9	.9
Beam diameter after scattering	0.24 cm	1.0 cm

Figure 7.2 shows a plot of the key nozzle and gas parameters as a function of position, as determined by Princeton. Figure 7.3 shows a blowup of the energy deposition profile.

After several iterations, we concluded that we needed a field which converges to 200 kG at z = 5 cm in order to keep the beam from hitting and heating the nozzle wall near the throat. The equation for the field strength was:

$$B = (200\ \text{kG})\left(\frac{20\ \text{cm}}{z\ +\ 15\ \text{cm}}\right)^2 \qquad (7.1)$$

In addition, the beam diameter needed to be about 1.0 cm at the z = 1.0 m location. So the total configuration requires that the beam enter the nozzle at a shallow angle following a 3-kG field. The beam remains small as it is guided down the nozzle on the axial centerline. At z = 1.0 m, the field begins to increase until it reaches 200 kG at z = 5 cm.

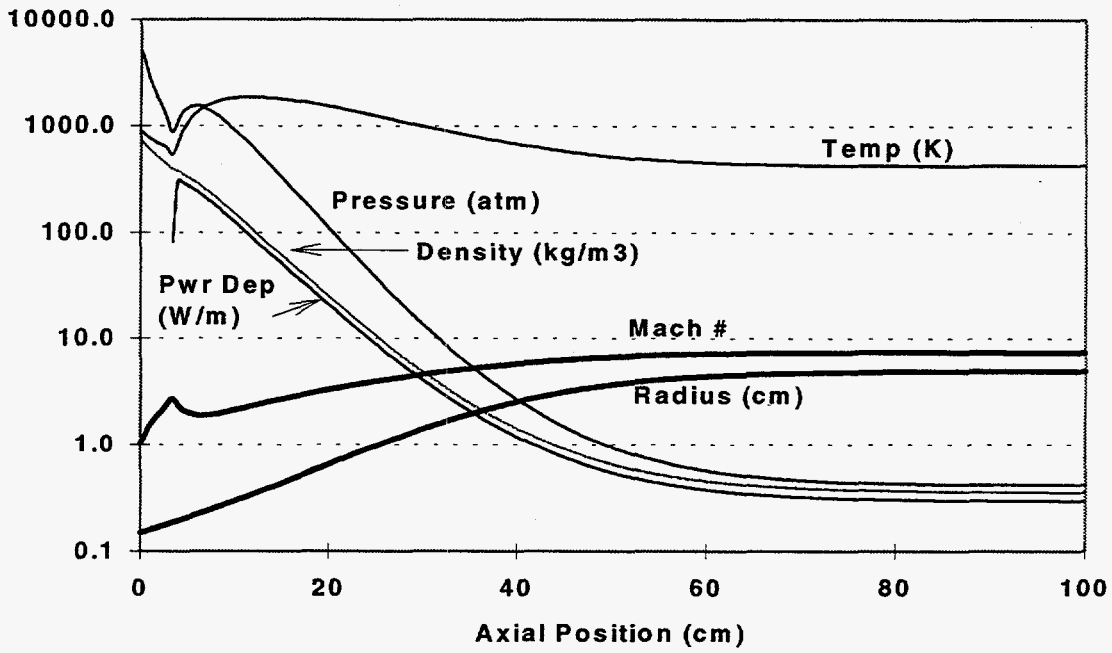

Figure 7.2. Nozzle and gas parameters for a pilot-scale wind tunnel with 21 MW of heating.

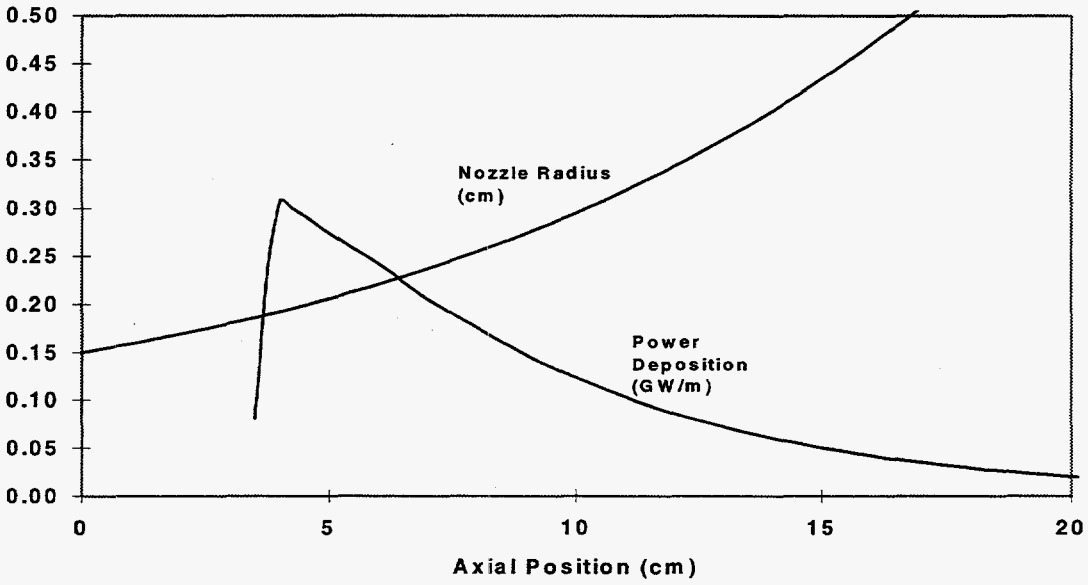

Figure 7.3. Energy deposition profile used by Princeton for the pilot-scale wind-tunnel.

Figure 7.4 shows the results for four selected electrons with this field, and Figure 7.5 show ten trajectories. (A total of 200,000 source electron trajectories were calculated in the simulation). The beam is fairly well confined for this configuration in spite of strong scattering

by the very dense air in that region. Figure 7.4 suggests that the major deposition occurs up to about z = 5.5 cm. This is very consistent with the Princeton modeling as shown in Figure 7.3.

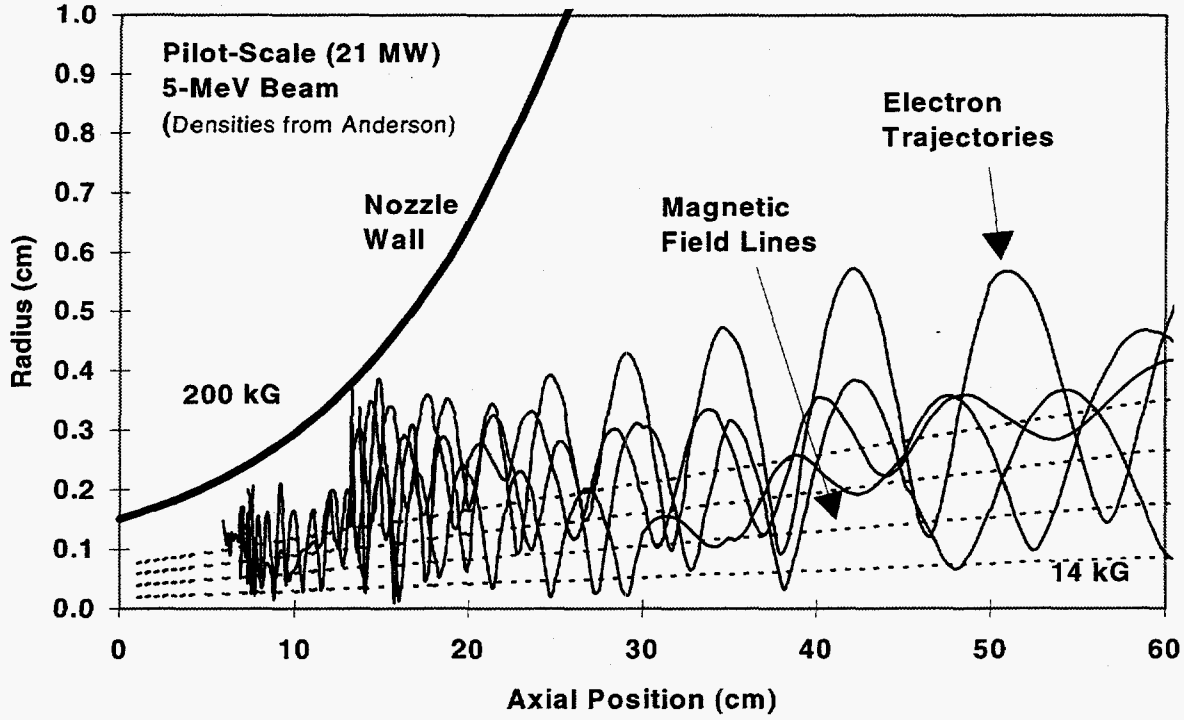

Figure 7.4. Four sample electrons following a field converging to 200 kG with nozzle radius and gas conditions taken from the Princeton design for a Mach-12 pilot-scale wind tunnel.

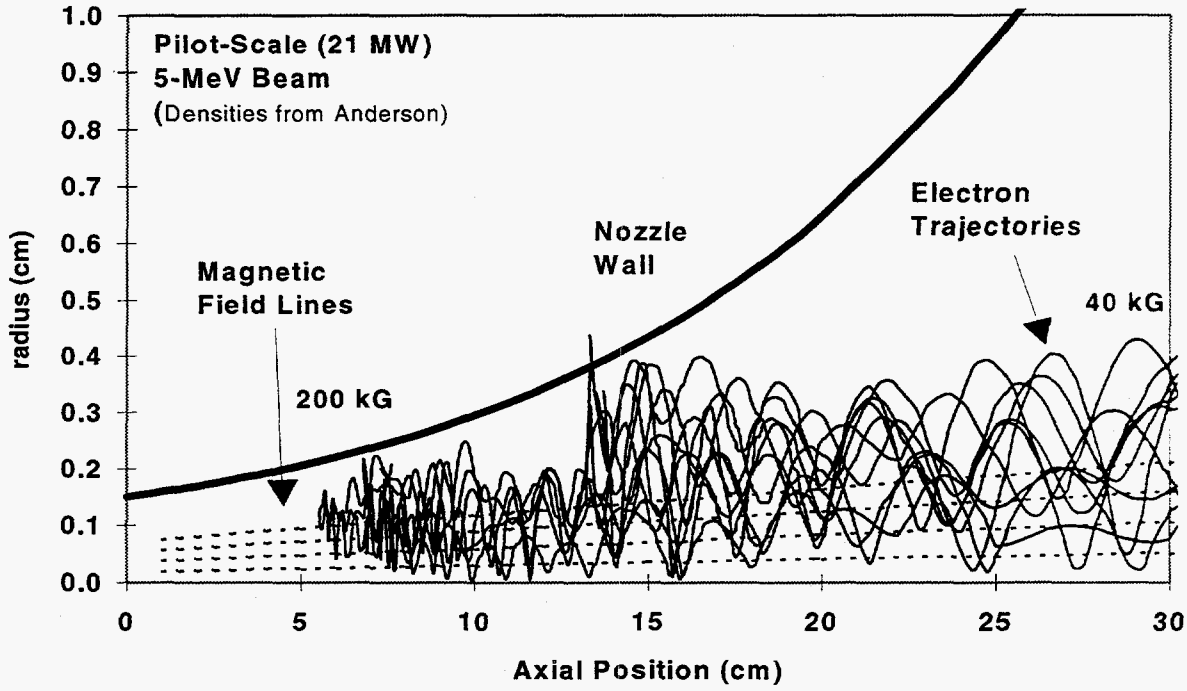

Figure 7.5. Ten sample electrons for the same conditions as in Figure 7.4, expanded horizontally.

A 200-kG field requires a very strong magnet. Sandia has already developed and demonstrated magnets in its coilgun program that are similar to what is required.[8] A series of 5 solenoidal coils linked together produced an axial field of 240 kG with a length of 27 cm and a diameter of 5 cm. This assembly was fired many times without coil damage. The power source limited the field duration to 0.15 ms, and temperature rises would be expected to limit the operation to about 2 ms if a stronger power source were used. However, moderate design changes would allow for convective cooling (possibly by transient boiling in small capillaries) which could extend this duration to the 1-second regime or higher.

Figure 7.6 shows the axial-profile for various radial locations. Note how the deposition rate per unit mass increases as the beam is compressed toward the throat, but at some point the electrons run out of energy and the deposition goes to zero (near 5 cm). Figure 7.7 shows the radial profile of the energy deposition rate for various axial locations. Note that the width of the energy deposition column decreases with decreasing z to match the convergence of the nozzle. Note also that very little energy is deposited in the nozzle walls.

Figure 7.8 shows the beam radius (at 1/e of maximum) vs axial position. The magnetic field keeps the beam well confined and away from the wall.

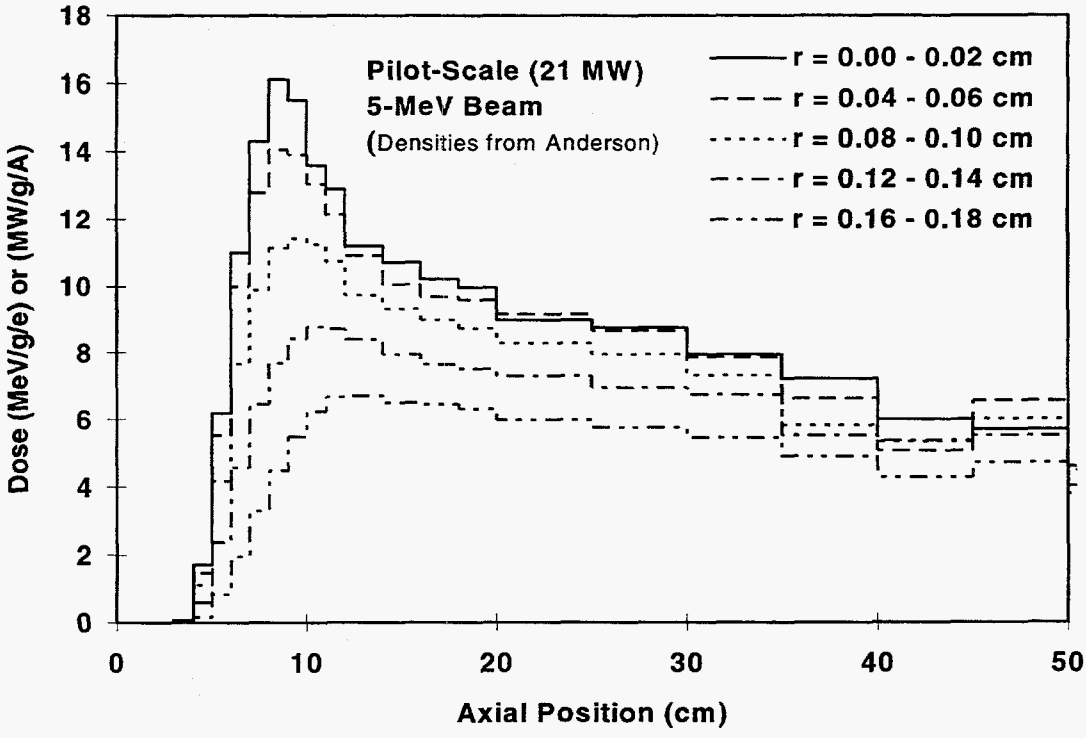

Figure 7.6. Axial profile of the energy deposition rate for various radial locations

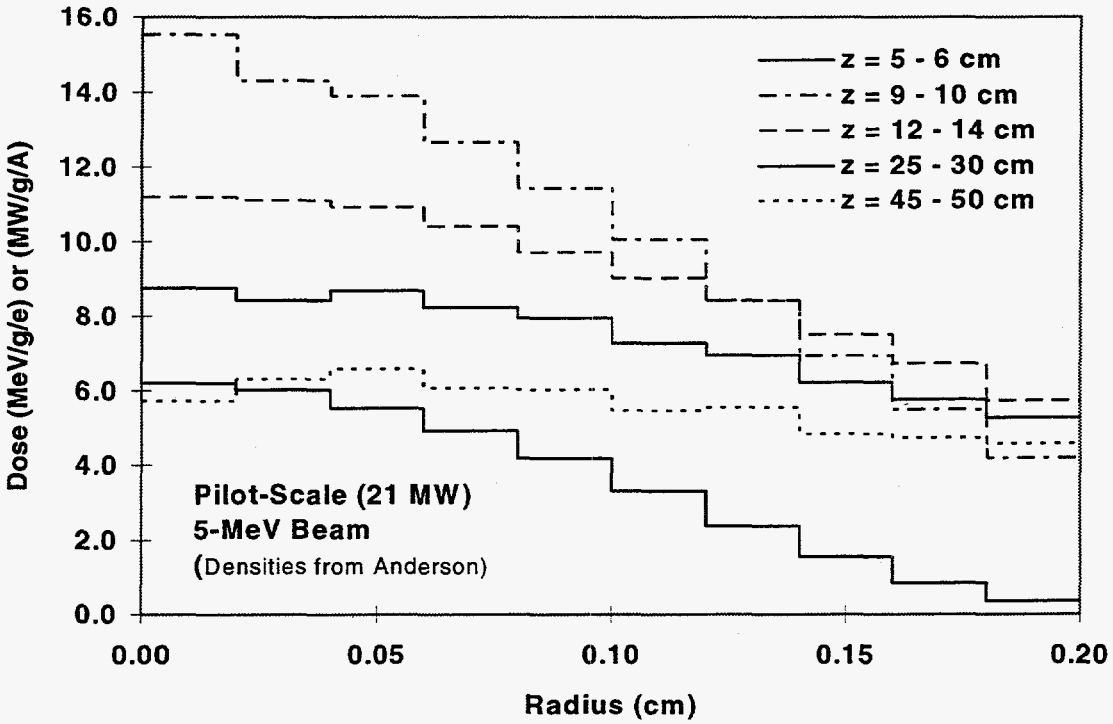

Figure 7.7. Radial-profile for various axial locations

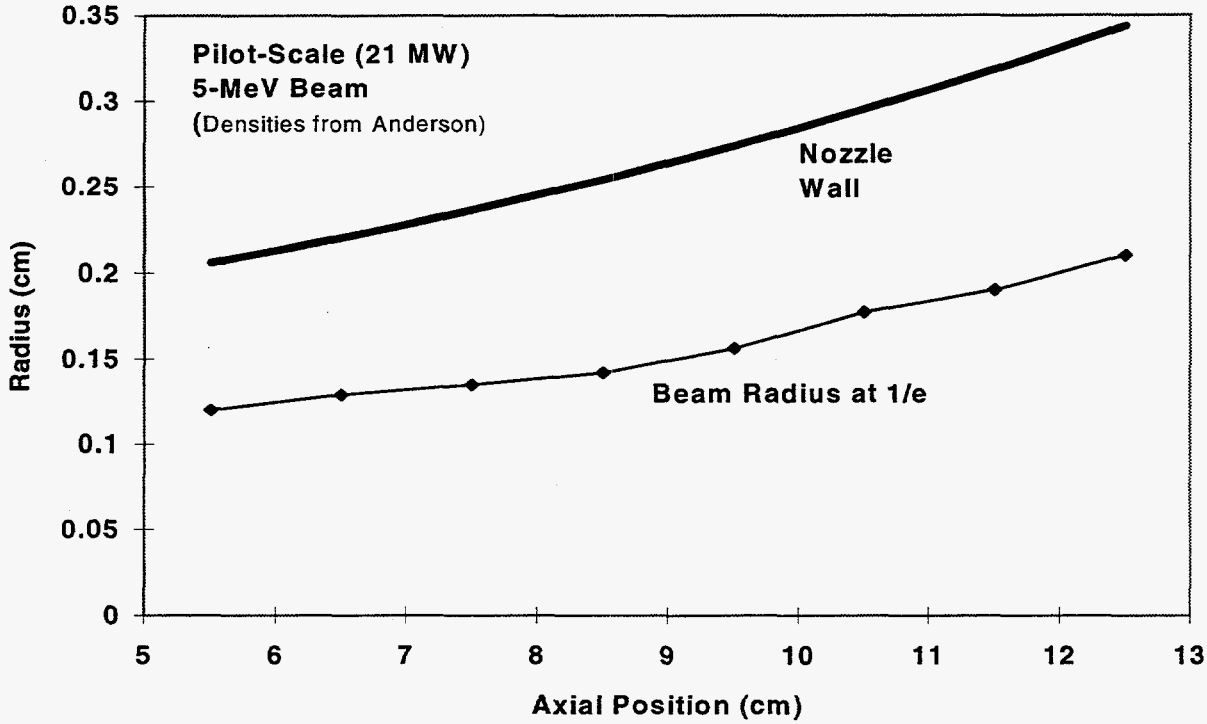

Figure 7.8 Beam radius (at 1/e of maximum) vs axial position.

8. Gas Chemistry Induced by the E Beam

A brief assessment was made on how electron-beam heating might affect the chemistry of the heated air. The electron beam deposits energy into the gas primarily by direct impact of the bound electrons in the gas molecules. (For 5-MeV electrons in air, about 2.2% goes into the production of Bremsstrahlung x rays.) Most of these impacts cause ionization of the molecule, and some cause simultaneous dissociation. The ejected electron is typically many keV in energy, and it goes on to ionize or excite more molecules. The net result is a cascade of electrons which eventually results in a plasma with electron energy comparable to the ionization potential of the gas molecules or atoms.

This plasma co-exists with the neutral gas at a number density determined by the ionization rate and the recombination rate. At the same time, ion chemistry and neutral chemistry is proceeding at rates dependent on the number density of the various species and the gas temperature. The beam energy is eventually converted to heat as recombination and chemical reactions yield excited vibrational states, and subsequent collisions transfer this energy to translational energy. This total process is very challenging to model completely.

Experimental data show that electrons in the MeV regime lose an average of 32.5 eV for every ion produced.[9] Since the average ionization energy for air (without dissociation) is 14.9 eV, most of the remaining energy is in the kinetic energy of the free electrons or in excited states of the atoms or molecules. The low-energy electrons also are available to excite the molecules without ionizing them. For the base case, the gas flow is 79 kg/s, and the added energy is 400 MW. The fraction of gas that undergoes ionization is thus

$$f_i = \frac{P_b m_{am}}{E_i w_g} = \frac{(400 \times 10^6 \text{ W})\ (4.81 \times 10^{-26} \text{ kg})}{(32.5 \times 1.6 \times 10^{-19} \text{ J})\ (79 \text{ kg/s})} = 0.047 \qquad (8.1)$$

where P_b is the beam power, m_{am} is the average mass of an air molecule, E_i is the average energy per ion pair produced, and w_g is the total gas mass flow rate. So only about 5% of the gas goes through an ionization and recombination process, primarily as it passes through the zone from 0.5 to 1.0 m down the nozzle. At the high densities in the heated region, recombination will be quite fast. A detailed code is needed to track the ionization, recombination, and air chemistry.

The Computational Optical and Discharge Physics Group (CODPG) at the University of Illinois has developed a suite of computer models which address electron beam excitation and plasma chemistry of high pressure plasmas.[10] These codes were originally developed for e-beam excitation and fission fragment excitation of excimer and rare gas lasers; and for electric discharge excited air plasmas for toxic gas remediation.

The computer code WVALUE is a Monte Carlo simulation of the slowing of an electron beam in an arbitrary gas mixture. The user specifies the mole fractions, pressure and temperature of the gas mixture of interest. WVALUE then accesses an online electron impact cross section data base, WVXSECS, to obtain the necessary transport coefficients. WVALUE produces the

electron energy distribution, "W-values", excitation rates and energy partitioning for all pertinent electron impact processes. This information can be generated as a function of position from the foil for single or double sided pumping. WVALUE also contains a Boltzmann solver using the 2-term spherical harmonic expansion method, and so can address electron-beam sustained discharges.

Three computer models have been developed to address high pressure plasma chemistry. All use general "Chemkin-like" input files to specify species and reactions. KRFDIS was originally developed to address high pressure electron beam and discharge excited KrF lasers. FFLASER was originally written to address fission fragment excitation of rare gas lasers. TOXIC was originally developed to address atmospheric pressure discharge excited plasmas for toxic gas cleanup. All models are time dependent, zero-dimensional codes.

University of Illinois modeled the chemical interactions for the large-scale wind tunnel described previously.[11] Unfortunately, a fully self-consistent set of input conditions in which the nozzle expansion was matched precisely to the axial energy deposition by the e-beam was not available. So we used the nozzle and gas conditions for the case of laser-heated gas instead (reference 1). U. of Illinois then simulated an electron beam penetrating that configuration of gas density, temperature, and velocity, and determined the resulting chemical compounds as the gas flowed down the nozzle. The match between beam-energy deposition and gas temperature rise (or enthalpy rise) was not correct as a function of axial position, but the total energy added was correct, and the results are a good first estimate of the expected chemistry.

Figure 8.1 shows the energy deposition vs. axial position in the nozzle. The deposition tail extends further upstream than it should because of a modeling approximation, but the difference from a more precise simulation is not very consequential. Figures 8.2 through 8.5 show how rapidly the ions neutralize, including the dominant ion O_2^- which is formed by electron attachment. Essentially all of the ionization is gone by the time the gas has flowed to the 3-meter point.

Figures 8.6 and 8.7 show how the neutral gas chemistry evolves as the gas flows and expands, with Figure 8.7 displaying the constituents in terms of mole fraction. After about 3 meters, the constituents "freeze" into place and change very little thereafter because of the low gas densities downstream. The levels of NO and NO_2 end up at about 0.08%. These levels are much lower than we had initially thought would be the case for e-beam heating.

The intent of heating the gas in the nozzle is to achieve exit temperatures which are prototypic of the upper atmosphere, but avoid having non-prototypic chemistry caused by excessively high temperatures in the initial plenum. Without heating in the nozzle, the plenum temperature would have to be about 6300 K, and the NO and NO_2 concentrations would be about 10% and 1%, respectively. So the low concentrations levels shown by the calculations for e-beam heating (less than 0.1% each) suggests that post-heating the gas with an e beam is a major step forward in producing prototypic air conditions. The levels are not as low as with laser heating, but they are probably more than adequate for wind-tunnel applications because NO and NO_2 levels comparable to these are expected to be created when the air is compressed as it enters

a hypersonic air-breathing engine.

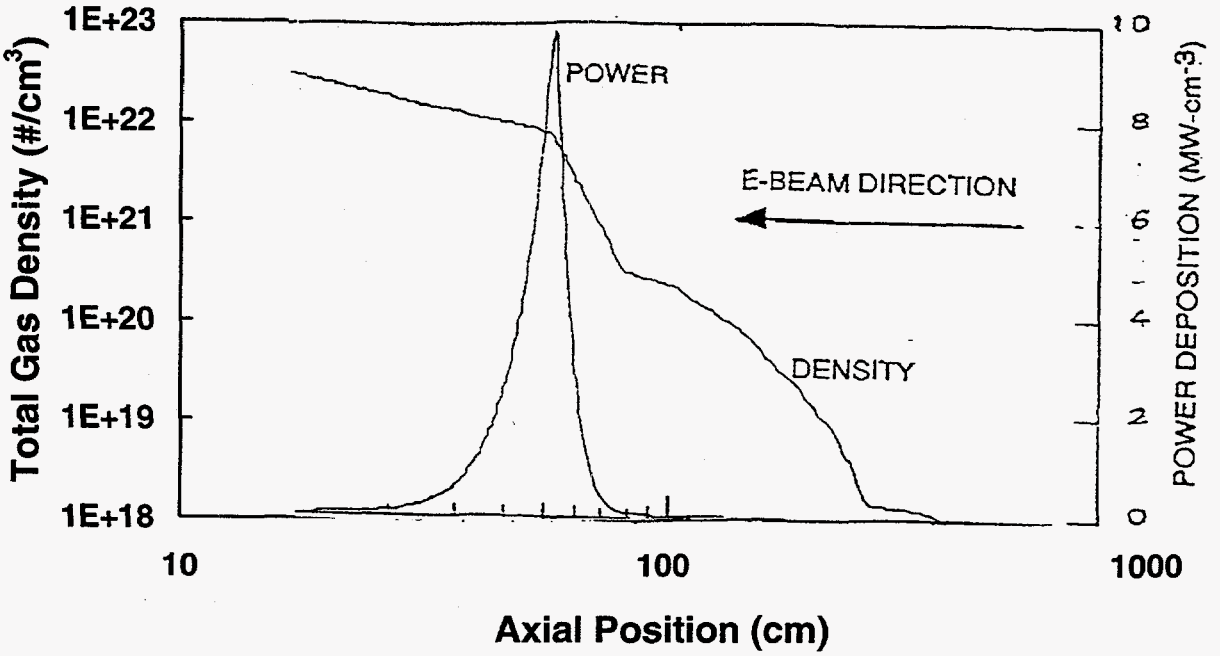

Figure 8.1 Energy deposition vs. axial position in the nozzle used in the chemistry simulations

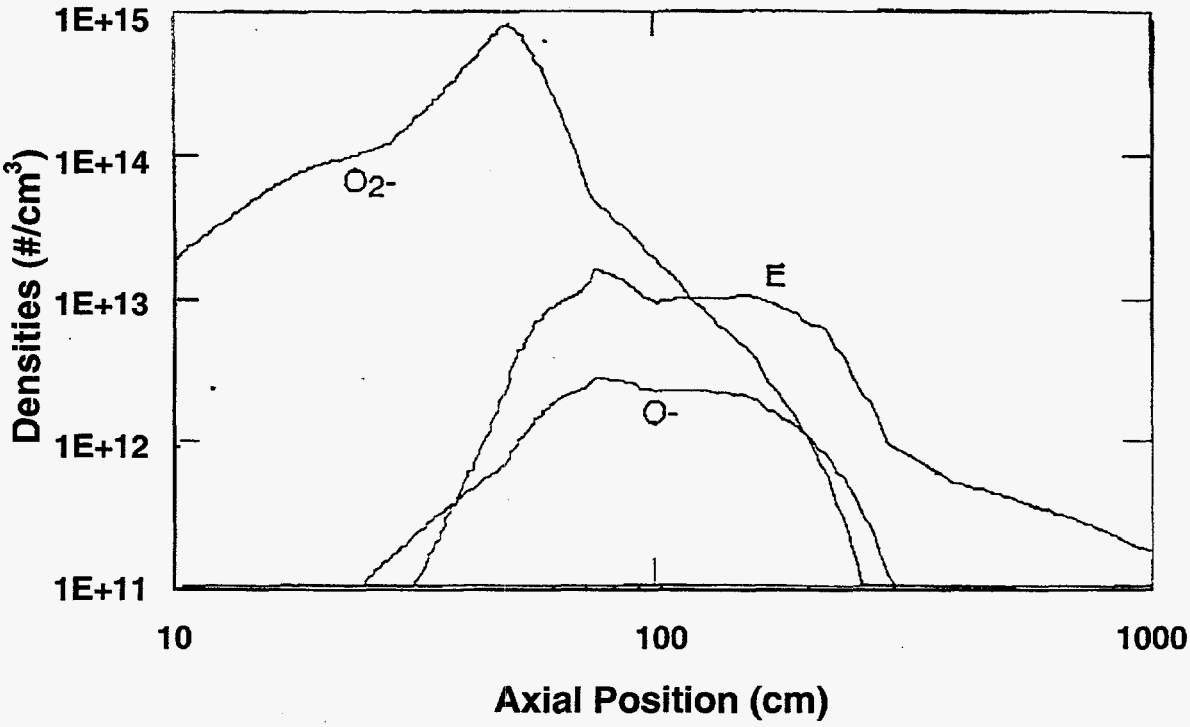

Figure 8.2 Densities vs. axial position for electrons, O^-, and O_2^-

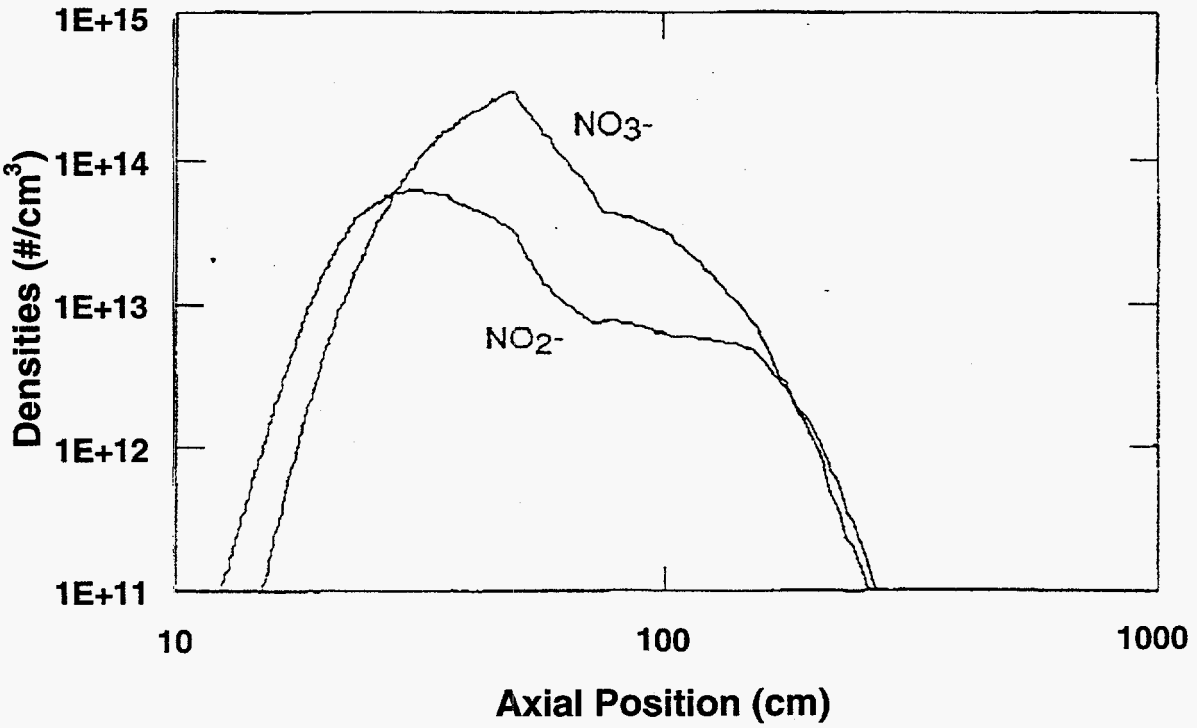

Figure 8.3 Densities vs. axial position for NO_3^- and NO_2^-.

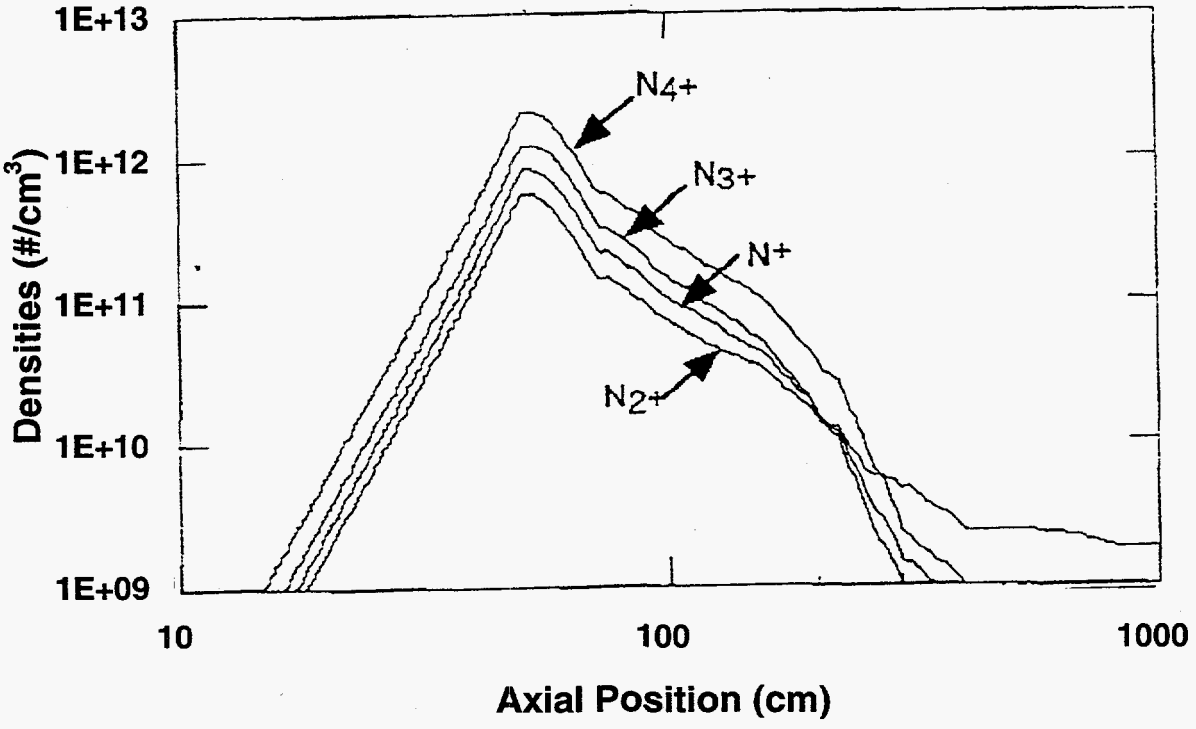

Figure 8.4 Densities vs. axial position for N_4^+, N_3^+, N^+, and N_2^+.

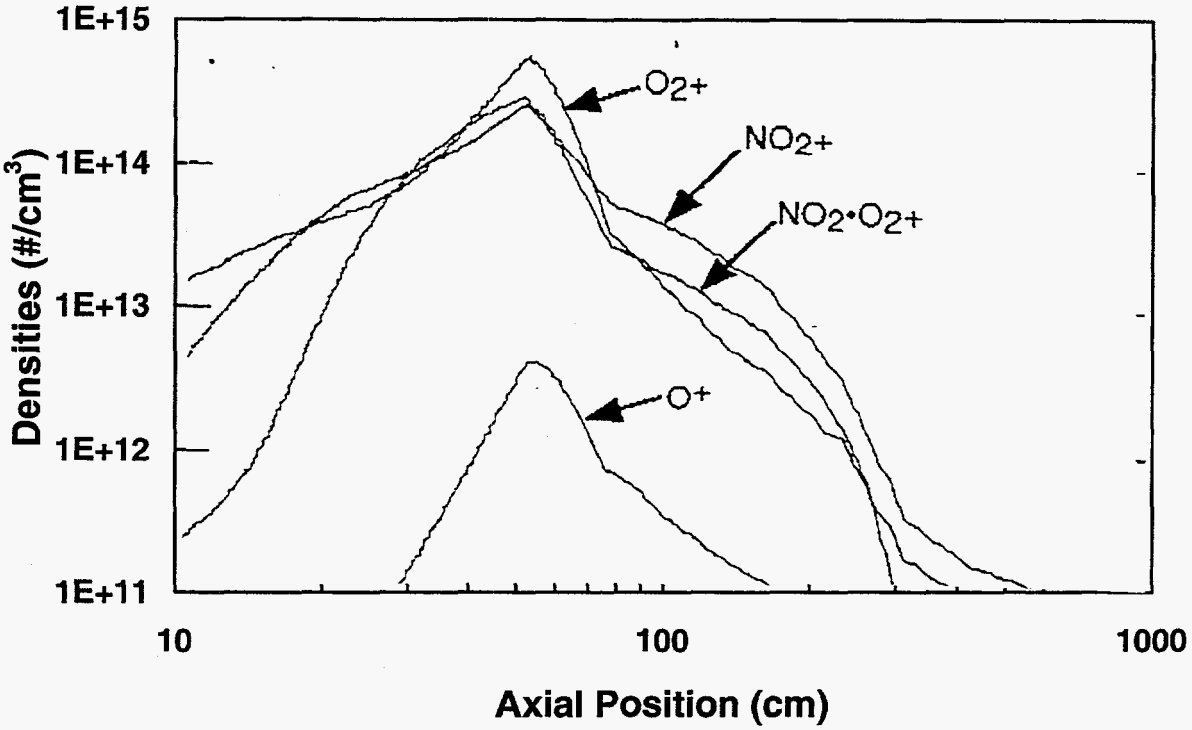

Figure 8.5 Densities vs. axial position for O_2^+, NO_2^+. NO_2-O_2^+, and O^+.

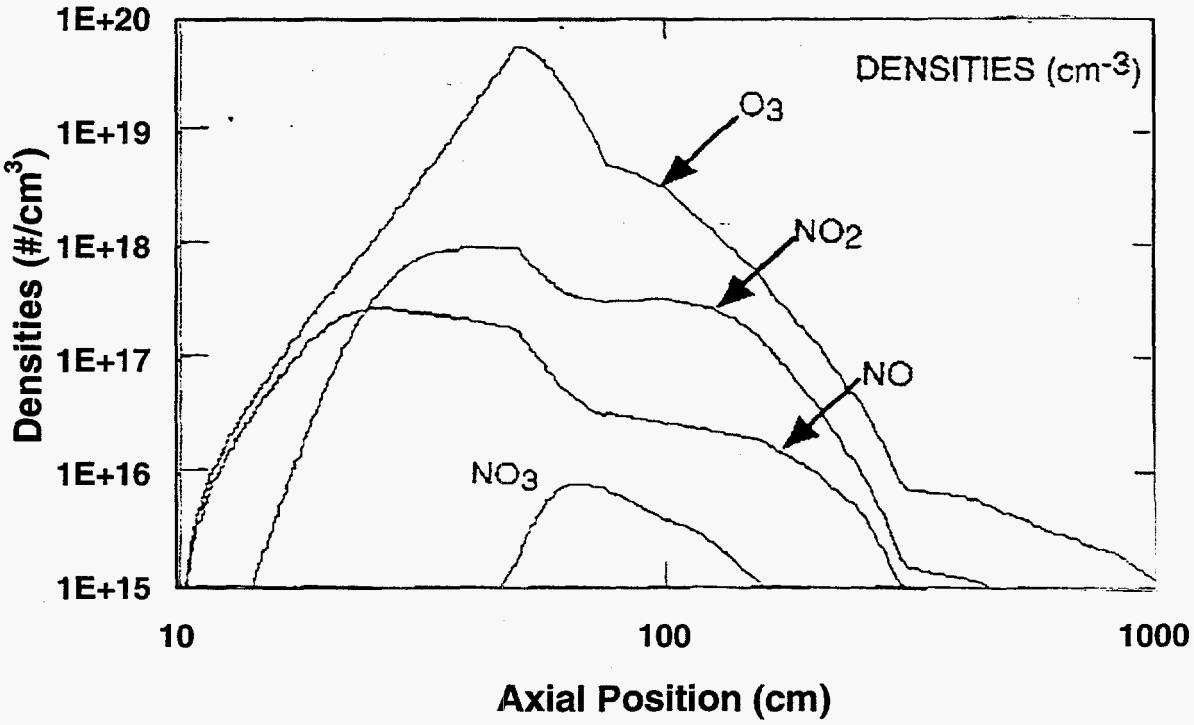

Figure 8.6 Densities vs. axial position for O_3, NO_2, NO, and NO_3.

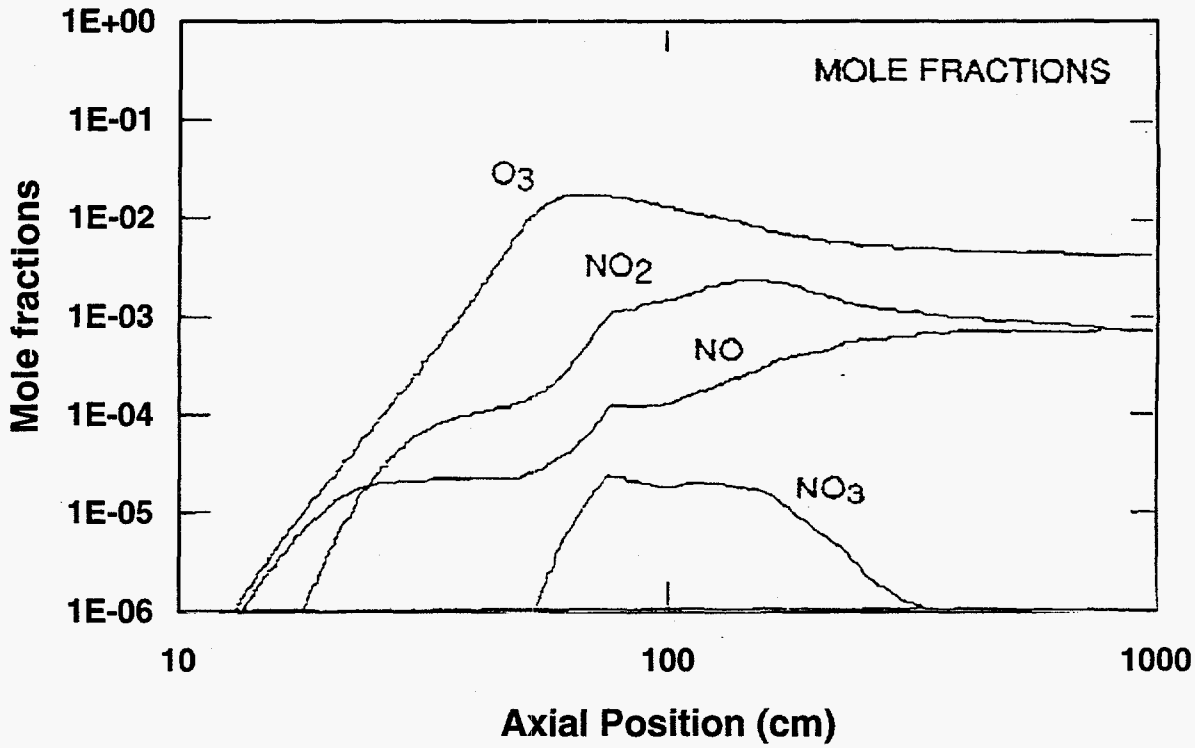

Figure 8.7 Mole fraction vs. axial position for O_3, NO_2, NO, and NO_3.

9. Accelerator and Power Supply

The accelerator for the large-scale system is a "DC" accelerator composed of a Marx capacitor bank and an electrostatic beam source (referred to as a "diode"). It is similar to the Troll accelerator at Sandia National Laboratories[12] except it is slightly higher voltage and much longer in beam duration, and delivers a lower current. The Troll accelerator (Figure 6.2) can produce about 1000 A at 4 MeV for 1 microsecond; the wind-tunnel accelerator is designed for 90 A at 5 MeV for 0.1 seconds. The most significant difference is the much longer beam duration.

The accelerator works by establishing a constant (DC) voltage of 5 MV across a single large acceleration gap. The voltage is established by first charging a large bank of capacitors to 50 kV in parallel, and then rapidly reconnecting the capacitors in series to yield 5 MV. Such a system is called a "Marx" bank, and the reconnection process is called "erecting" the capacitor bank.

Figure 9.1 shows the general configuration for the Marx bank.[13] The 50 kV power supply slowly charges the bank through charge resistors with resistance R_c. A set of spark-gap switches connects the capacitors in series but are initially open. After the bank is charged, a few of the switches are closed by inducing a spark in them. An electric pulse then progresses and causes a breakdown in the remaining switches to close them all in rapid order. This erects the bank to a total voltage of 5 MV.

The bulk of the current is now delivered to the accelerator diode where it is absorbed by the 90-A e beam. However, some of the current is shorted out back through the charging resistors. The object of the design is to make these resistors small enough to charge the capacitors in a reasonable time, yet large enough cause negligible shorting during the 0.1-second beam time. These criteria are met for the conditions shown in Table 9.1 and are the design configuration for the accelerator.

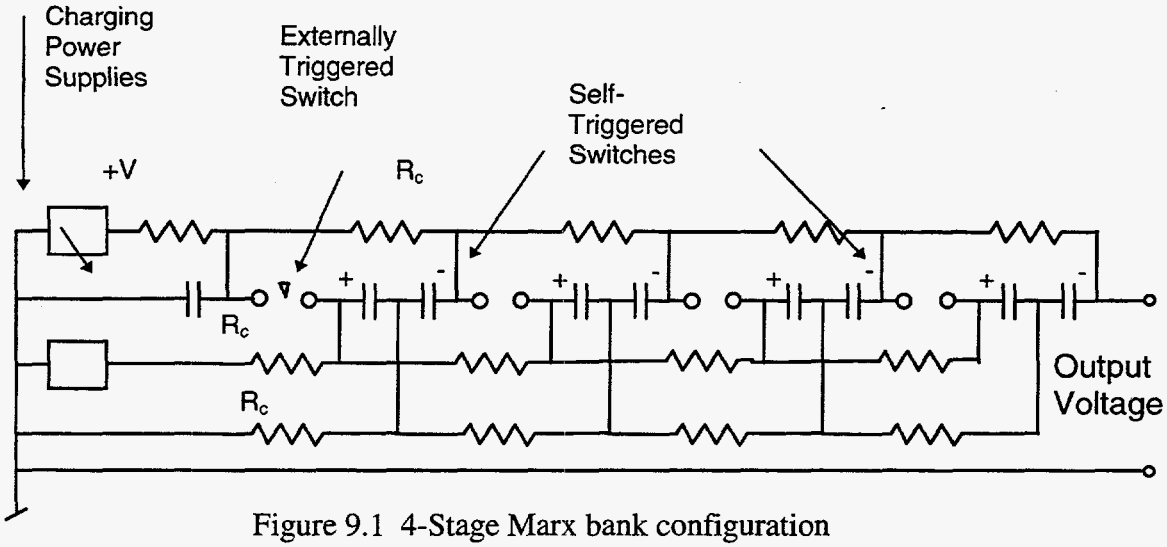

Figure 9.1 4-Stage Marx bank configuration

Table 9.1 Capacitances and resistances for the accelerator Marx bank.

Item	Large-Scale	Pilot-Scale
Charging voltage	±50 kV	±50 kV
Number of stages	50	50
Output voltage	5 MeV	5 MeV
Capacitor size	40 μF	40 μF
Capacitor energy	50 kJ	50 kJ
Total stored energy needed	100 MJ	50 MJ
Total number of capacitors	2000	1000
Capacitors per stage	40	20
Charging resistance between stages	4 kΩ	80 kΩ
Isolation resistance to ground	4 kΩ	80 kΩ
Time constant for charging	640 s	6400 s
Time constant for bleedoff	0.8 s	11 s

The characteristic charging time is $t = 2 N_s R_c N_c C$, where N_s is the number of stages in the Marx, R is the resistance of each charging resistor, N_c is the number of capacitors per stage, and C is the capacitance of one capacitor. The characteristic time for bleed-off of the current

through the charging resistors after firing is $t = 0.17 R_c N_c C$ (if the beam-generating diode has infinite impedance). This time must be larger than the desired pulse duration. This leads to the requirement of rather large resistances in the charging circuit and long charge times (especially for the prototype machine which has a 1.0 second beam requirement). If these charge times are too long, an alternative solution is to insert mechanical opening switches (solenoids) between the charging resistors of each capacitor stage and open them when charging is complete. (This is often done on the power supply to protect it from high voltages when the Marx is fired).

Another requirement for the Marx bank is to resist surface breakdown for the duration of the beam. This is done by immersing the capacitors in transformer oil with adequate spacing between surfaces with large voltage differences. The experience with Troll shows how much spacing is adequate for a beam of several microseconds. There is some uncertainty on how much more is needed for a 0.1-s or 1.0-s beam. However, conventional wisdom is that there is not much difference between a microsecond and about 1 second in terms of the needed distances. This question can be easily resolved by a series of tests with just a few capacitors.

Commercial capacitors are available with a 50-kV, 50 kJ rating (40 microFarads). If we assume that we can deliver 45% of the stored energy to the beam, then we need a total of 100 MJ of capacitors, which is 2000 capacitors. However, in order to achieve this efficiency, we must shape the decay of the voltage on the capacitors to be more of a square wave than an exponential decay. This is done with a Guilleman circuit,[14] which is a set of capacitors and inductors placed between the Marx bank and the diode.

The DC voltage is delivered to an electrostatic diode to produce the 90-A e beam. The Troll accelerator uses a cold cathode made of velvet. The carbon (cloth) whiskers on the velvet experience a large electric field on their tips which cause them to explode into a plasma. This plasma then becomes the source for the electrons in the beam. Such a system works well on the microsecond time scale. However, the plasma will tend to expand at about 1 cm/microsecond, so this approach is probably not appropriate for a 0.1-s beam. We plan to use a thermionic (hot) cathode instead.

A hot cathode uses a heated metal as the source of electrons for the beam. There is no expanding plasma connect to ground and short out the diode. If this cathode is recessed properly inside a cavity, fringe fields will help keep the resulting beam focused. Hot cathodes can generate up to 10 A/cm^2, so we plan to use 25 cm^2 with about 4 A/cm^2. Hot cathodes also require a very good vacuum when operating, so care must be taken in designing the entrance of the beam into the wind-tunnel nozzle. This will be discussed shortly.

The barrier (interface) between the Marx oil insulation and the diode vacuum must avoid surface breakdown for the duration of the beam. This is accomplished by making a long path from the negative surface to the positive surface, and by making a series of angled steps on the insulator stack so that electrons leaping from the insulator surface are trapped before they can accumulate much energy.

The typical distance that can be supported in the microsecond regime is about 3 MV/m, and this is the design basis used in the Troll accelerator. Again, there is uncertainty over how much more distance is needed for a 0.1-s beam. However, conventional wisdom says that not much more is needed, and experience with 20-MV Van de Graaff accelerators confirms this. So the wind-tunnel accelerator design uses 5 meters for 5 MV, but it might be able to handle the voltage with only 2 meters of insulator stack. Again, this question can be resolved by testing before the design is finalized..

The beam enters the wind-tunnel nozzle through a small open port so that we can avoid melting the nozzle wall. Fortunately, this is at the low-pressure end of the nozzle, but we still must use a careful design and strong differential pumping to protect the hot cathode from too much gas. The approach used was shown in Figure 6.1.

The nozzle is initially evacuated. When operation begins, the air enters nozzle and reaches a maximum pressure of 0.0015 atmospheres. To reach the cathode, the air must first pass through a long small-diameter tube. The tube is pre-cooled to cryogenic temperatures, so any air molecules which hit the walls will tend to condense out. The tube also is slightly "S" shaped so that there is no direct path through it.

Any air which survives passage through the tube then enters a large blowdown tank. This tank also has cryogenically-cooled panels in it. Furthermore, to reach the cathode, the air must make another turn and go through a small hole in the wall of the blowdown tank. Only a very small fraction of the air will survive this path without condensing on the cooled walls and plates. These also is a fast-closing valve to seal off the diode region after the beam has finished passing (0.1 s).

Magnetic fields are used to guide the beam through the blowdown tanks and into the wind-tunnel nozzle. A transverse field is used to bend the beam over short distances, and an axial field is used to confine it over long distances. The strengths of the fields indicated in Figure 7.1 are designed to yield the proper radii of curvature and confinement.

An alternative design for differential pumping is to use several tanks in succession and eliminate the need for cryopanels. (See Figure 9.2). The pressure buildup in each tank increases linearly at first and is proportional to the area of the entrance tube divided by the volume of the tank. If we assume sonic velocity in each entrance tube and that the connecting tubes are such that air cannot stream directly from one tank to another without bouncing off the walls, then the rate of pressure change in the n^{th} tank initially is

$$\frac{dP_n}{dt} = \frac{A_t v_s}{V_t} \frac{P_{n-1} T_n}{T_{n-1}} \qquad (9.1)$$

This is valid for $t << V_t / (A_t v_s)$.

For times as short as this, the pressure in the n^{th} tank is then approximately

$$P_n = \left(\frac{A_t v_s t}{V_t}\right)^n \left(\frac{T_n}{T_0}\right) \frac{P_0}{n!} \qquad (9\text{-}2)$$

where A_t is the cross-sectional area of each tube connecting the tanks, v_s is the speed of sound, t is time, V_t is the volume of each tank, T_n is the gas temperature at tank n (allowing for cooling from expansion), T_0 is the gas temperature in the wind tunnel, and P_0 is the pressure in the wind tunnel.

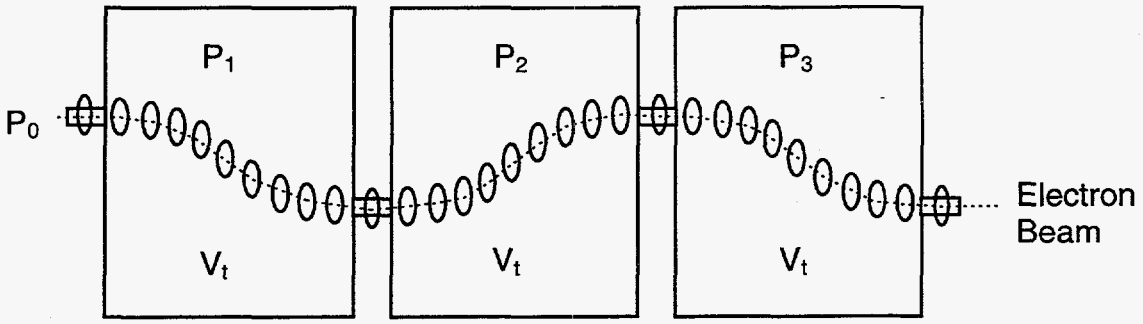

Figure 9.2. Series of tanks for differential pumping. A series of short solenoids guides the e beam from one tank to the next.

For example, if the connecting tubes are each 8 cm in diameter, and the volume of each tank is 100 m^3, v_s = 300 m/s, and if we ignore the temperature drop from cooling, then at t = 0.1 seconds the pressure is attenuated by a factor of about 1000 for each tank. Thus only two tanks are needed to drop the pressure from 1 Torr in the wind tunnel nozzle down to 10^{-6} Torr just outside the accelerator. If we want to go for 1.0 seconds, we would need three tanks.

10. Cost Estimates

The cost of the e-beam system was roughly estimated at this point. The e-beam system consists of the accelerator, beam injection hardware, vacuum pumps, numerous solenoidal and steering magnets, beam data acquisition system, and control systems for the beam and accelerator. Experience with accelerator and magnetic systems shows that the costs are dominated by the accelerator. The accelerator cost scales with the capacitor cost in the Marx generator. The remaining hardware is a fairly simple extrapolation of existing systems. Table 10.1 gives a summary of the component costs for the e-beam system.

The cost of the pilot-scale e-beam system was roughly estimated at this point. The e-beam system consists of the accelerator, beam injection hardware, vacuum pumps, numerous

solenoidal and steering magnets, beam data acquisition system, and control systems for the beam and accelerator. Experience with accelerator and magnetic systems shows that the costs are dominated by the accelerator. Table 10.2 gives a summary of the component costs for the e-beam system. It may be possible to reduce this cost by building several small accelerators and firing them in sequence.

Table 10.1. Rough cost estimate for the 450-MW, 0.1-s, e-beam system used to heat a Mach-14 large-scale hypersonic wind tunnel.

100 MJ of Marx banks @ $0.25/J	$25 M
Diode and remainder of accelerator	$25 M
Magnets & power supplies	$15 M
Pumps & tanks	$ 5 M
Diagnostics & control	$ 5 M
Labor (development & assembly)	$20 M
Total	$95 M

Table 10.2. Rough cost estimate for the 25-MW, 1-s, e-beam system used to heat a Mach-12 pilot-scale hypersonic wind tunnel.

50 MJ of Marx banks @ $0.25/J	$13 M
Diode and remainder of accelerator	$15 M
Magnets & power supplies	$8 M
Pumps & tanks	$ 5 M
Diagnostics & control	$ 5 M
Labor (development & assembly)	$17 M
Total	$65 M

11. Conclusions

Heating wind-tunnel air with an axial e beam may be an excellent and viable alternative to using laser beams. The accelerator and guiding magnetic fields would almost certainly be less expensive than a laser. In addition, beam propagation may be more tractable for electrons on magnetic field lines because a laser beam will greatly disturb the index of refraction of its medium. An e beam is less susceptible to causing wall damage than a laser beam because the energy is deposited in depth, not on the surface. It is recommended that this option be considered further.

12. References

[1] R. Miles, G. Brown, W. Lempert, D. Natelson, R. Yetter, J. Guest, G. Williams, and S. Bognonoff, "Radiatively driven hypersonic wind tunnel," *18th AIAA Aerospace Ground Testing Conference, June 20-23, 1994, Colorado Springs, CO*, AIAA-94-2472 (1994).

[2] R. B. Miles, G. L. Brown, W. R. Lempert, R. Yetter, G. J. Williams, and S. M.Bognonoff, D. Natelson, J. R. Guest,"Radiatively driven hypersonic wind tunnel," AIAA Journal, V. 33, N. 8, pp. 1463-1470, August 1995

[3] L. Pages, E. Bertel, H. Joffre, and L. Sklavenitis, *Atomic Data, v4*, pp 1-127 (1972).

[4] P. W. Werner, E. Schamiloglu, J. R. Smith, K. W. Struve, and R. J. Lipinski, "Erosion of a Relativistic Electron Beam Propagating in a Plasma Channel," *Phys. Rev. Letters, v7, n.22,* pp 2986-2989, November 1994.

[5] A. H. Bushnell, Y. G. Chen, J. Shannon, and R. Clark, "Troll: A 4-MV peak voltage pulser," *MLR-2720, IEEE paper* (1988).

[6] R. J. Kaye, I. R. Shokair, R. W. Wavrik, J. F. Dempsey, W. E. Honey, K. J. Shimp, and G. M. Douglas, "Design and Evaluation of Coils for a 50-mm Diameter Induction Coilgun Launcher," *7th Symposium on Electric Launch Technology, April 20-24, 1994, San Diego, CA*, 1995

[7] R. Anderson, Princeton University, Princeton, NJ, personal communication, Nov 22, 1996.

[8] R. J. Kaye, I. R. Shokair, R. W. Wavrik, J. F. Dempsey, W. E. Honey, K. J. Shimp, and G. M. Douglas, "Design and Evaluation of Coils for a 50-mm Diameter Induction Coilgun Launcher," *7th Symposium on Electric Launch Technology, April 20-24, 1994, San Diego, CA*, 1995

[9] R. D. Evans, *The Atomic Nucleus*, pg 587, McGraw-Hill, New York, NY, 1955

[10] M. Kushner, University of Illinois, Urbana, IL, personal communication, September 16, 1996

[11] M. Kushner, University of Illinois, Urbana, IL, personal communication, September 16, 1996

[12] A. H. Bushnell, Y. G. Chen, J. Shannon, and R. Clark, "Troll: A 4-MV peak voltage pulser," *MLR-2720, IEEE paper* (1988).

[13] S. Humphries, Jr., *Principles of Charged Particle Acceleration,* John Wiley & Sons, New York, p. 237 (1986).

[14] Op cit previous Reference, p. 257.

DISTRIBUTION:

AEDC/DOT
Attn: Mr. Ron Bishel (2)
1099 Avenue C
Arnold AFB, TN 37389-9011

AEDC/DOT
Attn: Mr. Robert T. Crook (5)
1099 Avenue C
Arnold AFB, TN 37389-9011

Princeton University
Dept. of Mechanical & Aerospace Engineering
Attn: Dr. Walter Lempert
Engineering Quad, Room D414
Princeton, NJ 08544

Princeton University
Dept. of Mechanical & Aerospace Engineering
Attn: Professor Richard B. Miles (15)
Engineering Quad, Room D414
Olden St.
Princeton, NJ 08544

Wright Patterson Air Force Base
Attn: Mr. W. Lee Bain, II
Wright Laboratory-POPS
Building 18
1950 Fifth Street
Dayton, OH 45433-7251

Wright Patterson Air Force Base
Attn: Dr. Alan Garscadden
Air Force Wright Aeronautical Labs
AFWAL/POOC-3
Building 450
Dayton, OH, 45433

Wright Patterson Air Force Base
Attn: Dr. Keith Richey
Director of Plans
Building 45
2130 8th Street, Suite 1
Dayton, OH 45433-7542

Wright Patterson Air Force Base
WL/FIMO, Building 24C
Attn: Mr. Norman Scaggs (5)
2145 Fifth St., Suite 1
Dayton, OH 45433-7005

Wright Patterson Air Force Base
WL/FIMC, Building 450
Attn: Dr. George Seibert (2)
Chief, Computational Fluid Dynamics Branch
2645 Fifth St., Suite 7
Dayton, OH 45433-7913

Department of Energy
AL/STTD/WFO-MT
Attn: Mr. Bernard Whitaker
Albuquerque, NM

NASA Langley Research Center
Attn: Dr. Dennis M. Bushnell (2)
Associate Chief
MS 197
Hampton, VA 23665-5225

NASA Langley Research Center
Attn: Dr. Wayne D. Erickson
Chief Scientist
Hypersonic Vehicles Office
MS 353
Hampton, VA 23681

University of Illinois
Attn: Professor Mark Kushner (2)
Dept. of Electrical & Computer Engineering
1406 W. Green Street
Urbana, IL 61801

John Hopkins University
Attn: Dr. Frederick S. Billig
Applied Physics Laboratory
John Hopkins Road
Laurel, MD 20723-6099

Point Loma Industries
Attn: Dr. Leonard F. Buchanan
President and CEO
5910 Pacific Center Blvd.
Suite 200
San Diego, CA 92121

ANSER
Attn: Dr. Raymond L. Chase
1215 Jefferson Davis Highway
Suite 800
Arlington, VA 22202-3251

MicroCraft, Inc.
Attn: Dr. James Mitchell
Executive Vice President
P. O. Box 370
Tullahoma, TN 37388

Lawrence Livermore National Laboratory
Attn: Dr. Marc S. Costantino
MS L-353
P. O. Box 808
7000 East Avenue
Livermore, CA 94550

Lawrence Livermore National Laboratory
Attn: Dr. Richard More
MS L41
P. O. Box 808
7000 East Avenue
Livermore, CA 94550

Bolling Air Force Base
AFOSR/NA
Attn: Dr. Leonidas Sakell
Program Director
A-25, Building 410
110 Duncan Avenue
Washington, D.C. 20332-6448

Phillips Laboratory/LIDD
Attn: Dr. Concetto Giuliano
2550 Aberdeen Ave., S.E.
Kirtland AFB, NM 87117-5776

Naval Surface Warfare Center
Attn: Dr. Eric R. Hedlund
Chief Aerodynamicist
10901 New Hampshire Ave.
K24
Silver Spring, MD 20903

THE PENTAGON
Attn: Lt. Colonel Vince Albert
AF/TER
1650 Air Force
Washington, D.C. 20330-1650

NASA Ames Research Center
Attn: Dr. James O. Arnold
Chief
Space Technology Division
Moffett Field, CA 94035-1000

RAND
Attn: Dr. Natalie Crawford
Associate Director, Project Air Force
P. O. Box 2138
Santa Monica, CA 90407-2138

Los Alamos National Laboratory
Attn: Dr. Gregory H. Canavan
Senior Science Advisor
M.S. D434, Building SM30
Bikini Road
Los Alamos, NM 87545

1	MS 0825	W. H. Rutledge (9115)
1	MS 0836	C. W. Peterson (9116)
1	MS 1145	P. S. Pickard (9360)
10	MS 1146	R. J. Lipinski (9363) (10)
1	MS 1146	T. F. Luera (9363)
1	MS 1152	L. X. Schneider (9543)
1	MS 1153	M. T. Buttram (9323)
1	MS 1165	J. E. Powell (9300)
5	MS 1179	R. P. Kensek (9341) (5)
1	MS 1182	B. N. Turman (9521)
1	MS 1190	D. Cook (9500)
1	MS 9018	Central Technical Files (8940-2)
5	MS 0899	Technical Library (4916)
2	MS 0619	Review & Approval Desk (12690) for DOE/OSTI
1	MS 0161	Patent and Licensing Office (11500)